Petroleum Science
https://doi.org/10.1007/s12182-020-00514-1

ORIGINAL PAPER

Paleoenvironment and organic matter enrichment of the Carboniferous volcanic-related source rocks in the Malang Sag, Santanghu Basin, NW China

Tian-Jun Li[1,2] · Zhi-Long Huang[1,2] · Xuan Chen[3] · Xin-Ning Li[3] · Jun-Tian Liu[3]

Received: 8 April 2020 / Accepted: 24 July 2020

Abstract
Volcanic activity was quite frequent during the deposition of the Late Carboniferous Ha'erjiawu Formation in the Santanghu Basin. The petrology and organic and inorganic geochemical indicators were used to investigate hydrocarbon potential, paleoenvironmental conditions and organic matter enrichment of the mudstones. The results show that the oil generation capacity of the Ha'erjiawu Formation mudstones, which has abundant oil-prone organic matter (Type II kerogen with hydrogen index values mainly ranging from 250 to 550 mg HC/g TOC) in mature stage (T_{max} values mainly ranging from 435 to 450 °C), is considerable. The Ha'erjiawu Formation was deposited in a dysoxic, freshwater-mildly brackish, and warm-humid environment. During its deposition, the Ha'erjiawu Formation received hydrothermal inputs. The volcanic hydrothermal activities played an important role in the organic matter enrichment. In addition, the total organic carbon (TOC) is significantly positively correlated with the felsic mineral content, but it is negatively correlated with the carbonate mineral content and C_{27}/C_{29} ratios, indicating that terrigenous organic matter input also contributed to the primary productivity in the surface water. Therefore, the formation of the high-quality source rocks in the Ha'erjiawu Formation was jointly affected by the hydrothermal activity and the terrigenous organic matter input.

Keywords Organic-rich rocks · Paleoenvironment · Organic matter enrichment · Hydrothermal activity · Ha'erjiawu Formation · Santanghu Basin

1 Introduction

High-quality source rocks are generally characterized by high organic matter abundance and stable distribution, and they are also the material basis for the formation of large- and medium-sized oilfields (Magoon and Dow 1991; Qin 2015; Xiao et al. 2015; Li et al. 2017; Ghassal et al. 2018; Zhang et al. 2018). The development of high-quality source rocks is controlled by a variety of factors. The preservation conditions that favor the formation of high-quality source rocks mainly include an anoxic water column caused by geographical isolation, variations in the paleowater depth, or biological activity (Demaison and Moore 1980; Katz 1990). However, the paleoproductivity model mainly includes that the enrichment of organic matter due to high primary productivity in the surface water. As long as the paleoproductivity is high, even if the sedimentary water column is oxic, high-quality source rocks will develop under these conditions (Meyers and Arnaboldi 2005). The paleoproductivity of water columns mainly involves the contribution of lower aquatic organisms, terrigenous organic matter and hydrothermal activity in the water column. However, volcanic hydrothermally influenced organic matter accumulation has been highlighted during recent years. The formation of organic-rich rocks associated with hydrothermal activity has been reported in non-marine basins in China, especially the Lucaogou Formation in Santanghu Basin (Zhang

Edited by Jie Hao

✉ Zhi-Long Huang
huangzhilong1962@163.com

[1] State Key Laboratory of Petroleum Resources and Prospecting, China University of Petroleum (Beijing), Beijng 102249, China

[2] College of Geosciences, China University of Petroleum (Beijing), Beijing 102249, China

[3] Research Institute of Exploration and Development, PetroChina Tuha Oilfield Company, Hami, Xinjiang 839009, China

Published online: 27 November 2020

et al. 2018) and the Fengcheng and Lucaogou Formations in the Junggar Basin in northern and eastern parts of Xinjiang (Cao et al. 2015). Most scholars believe that volcanic eruption and volcanic ash promote algae/bacteria blooms, and volcanic eruption are accompanied by a large number of nutrient elements and the release of trace metals, which promote the primary productivity of the water column. This would cause organic matter enrichment in the sedimentary water column. Under the background of a volcanic eruption, the development of organic-rich mudstones can be divided into two stages: in the first stage, a large amount of volcanic matters falls into the water column in the early period of the volcanic eruption, resulting in the extinction of organisms. A large amount of hydrocarbon-generating parent material is rapidly accumulated and preserved, forming organic-rich mudstone, such as those in the Yincheng Formation in the Songliao Basin (Shan et al. 2013). The second stage is the late period of the volcanic eruption (the volcanic intermission), the volcanic ash in the atmosphere continues to fall into the water columns, resulting in a large bloom of algae and an increase in the primary productivity, such as in the Lucaogou Formation in the Santanghu Basin (Zhang et al. 2018) and the Fengcheng Formation and Lucaogou Formation in the Junggar Basin (Cao et al. 2015). The organic and inorganic geochemical characteristics of rocks can be used to evaluate the paleoproductivity of the water column (Ren et al. 2005; Kryc et al. 2003). The preservation conditions mainly include redox, acidity and salinity (Kendall et al. 2012). In addition, the lithology, mineral assemblage, and sedimentary facies indirectly reflect the preservation conditions of the organic matter (Zhang et al. 2018).

The commercial oil and gas obtained from many wells in the Ha'erjiawu Formation and its overlying strata (such as the Kalagang Formation) have been shown to be derived from the Ha'erjiawu Formation, the distribution range of which has an important effect on the hydrocarbon accumulation of Carboniferous volcanic rocks (Liu et al. 2015; Huang et al. 2012). During the deposition of the Late Carboniferous Ha'erjiawu Formation, multi-period tectonic movements and volcanic filling occurred (Liu et al. 2015). In such a complex structural and sedimentary background, thicker source rocks with a maximum organic matter abundance (total organic carbon; TOC) of 33% (average of 9%) were deposited in the Ha'erjiawu Formation (Li et al. 2018). It is well known that the development of high-quality source rocks is controlled by the paleoenvironment, such as paleoclimate, paleowater depth, redox conditions and paleosalinity. Semi-deep water to deep water environments characterized by dysoxic-anoxic, high salinity and warm-humid conditions are suitable for the development of organic-rich rocks (Zhang et al. 2018), whereas areas with strong tectonic movements and frequent volcanic activity are generally not suitable for the development of organic-rich rocks. Therefore, the factors controlling the high organic abundance of the source rocks in the Ha'erjiawu Formation still remain unclear. Moreover, there is a lack of detailed research on the relationship between their organic matter enrichment and sedimentary environment. Due to the limited drilling data, the sedimentary environment of the Ha'erjiawu Formation was mainly investigated from the geotectonic perspective. The results obtained from such studies are not always consistent. Wu et al. (2008) suggested that the Santanghu Basin was in an epicontinental sea-lagoon environment during the Late Carboniferous, while Wang et al. (2013a, b) suggested a lacustrine environment for the Santanghu Basin in the Late Carboniferous. In recent years, with the increasing amount of drilling data, Liu et al. (2011) determined the paleosalinity of the Ha'erjiawu Formation and reported that freshwater-brackish conditions prevailed during the deposition of the Ha'erjiawu Formation in the Santanghu Basin. However, the variations in the redox conditions, the paleoproductivity, and their effects on the organic matter enrichment were not comprehensively analyzed. Based on the results of previous studies and the regional tectonic setting, in this study, the paleoenvironment of the Carboniferous Ha'erjiawu Formation was reconstructed using the petrology, organic and inorganic geochemical indicators, and the relationship between the trace element ratios and the organic matter contents. Finally, we determined the main factors controlling the organic matter enrichment, which improve our understanding of the distribution of the high-quality source rocks in the Ha'erjiawu Formation. These results can also expand the new areas of deep oil and gas exploration in the Santanghu Basin.

2 Geological setting

The Santanghu Basin is located in the northeastern part of Xinjiang. Tectonically, it belongs to the suture zone of the Siberian Plate and the Kazakhstan Plate. The basin is rich in oil and gas resources and contains various reservoir types (Zhao et al. 2003). During the Middle Devonian-Late Devonian, the northward subduction of the Kalamaili oceanic crust of the Junggar Ocean formed a ditch-arc-basin system with active continental margins in the Santanghu area (Hu et al. 2020). The main body of the Santanghu area was an island arc environment. In the Late Devonian-Carboniferous, because of the subduction of the Kalamaili oceanic crust, the Junggar Block collided with Karamali on the southern edge of the Siberia Plate, and the oceanic crust disappeared, forming a residual basin with a small amount of seawater in the Santanghu area. A set of volcanic lava, volcanic clastic rocks and normal clastic rocks were deposited in this area. After this, due to the collisional orogeny, the seawater gradually retreated from the Santanghu area (Hu 1997; Wu

et al. 2008). In addition, Lin et al. (1997) suggested that in the late Carboniferous, the Santanghu area had an island arc environment in the post-plate collision stage, and there were large-scale volcanic eruptions and magma intrusions. Furthermore, the area of the Junggar Ocean decreased, and the residual seawater only existed in the southern part of the Santanghu area. Therefore, the Ha'erjiawu Formation may have residual seawaters between the closing of the ocean basin in the Early Carboniferous and a post-collisional, intracontinental, extensional setting in the Early Permian (Fig. 1). The basin can be divided into three first-order structural units: the northern uplift belt, the central depression and the southern thrust belt. The central depression belt can be divided into four bulges and five sags. The Malang sag is the main research area of this study (Fig. 2a). The basin experienced many tectonic movements, and the internal faults in the depressions are very well developed (Zhao et al. 2003). The main faults are northwest–southeast trending, and the secondary faults are northeast–southwest trending. Seven tertiary structures are present in the study area: The Mabei structure, the Niujuanhu structure, the Niudong structure, the Mazhong structure, the Madong structure, the Heidun structure and the Chaha structure (Sun et al. 2001; Lu et al. 2012) (Fig. 2b).

From bottom to top, the Carboniferous strata in the Malang Sag includes the Lower Carboniferous Jiangbastao Formation (C_2j), the Upper Carboniferous Batamayi Neishan Formation (C_2b), the Ha'erjiawu Formation (C_2h) and Kalagang Formation (C_2k) (Fig. 2c). The Jiangbastao Formation is a set of marine sediments. Its lithology is characterized by gray-black mudstone and gray sandstone. The Batamayi Neishan Formation is dominated by intermediated-mafic volcanic rocks (Hu 1997). During the deposition of the Ha'erjiawu Formation, the basin was in a compressional environment and experienced frequent volcanic activity. A set of volcanic rocks intercalated with mudstones, oil shales and tuff mudstones were developed in the basin during the intermission of volcanic eruption. The Kalagang Formation contains intermediate-mafic volcanic rocks intercalated with thin layers of volcanic clastic rocks and clastic rocks (Liu et al. 2009). The Carboniferous Ha'erjiawu Formation is the target of this study.

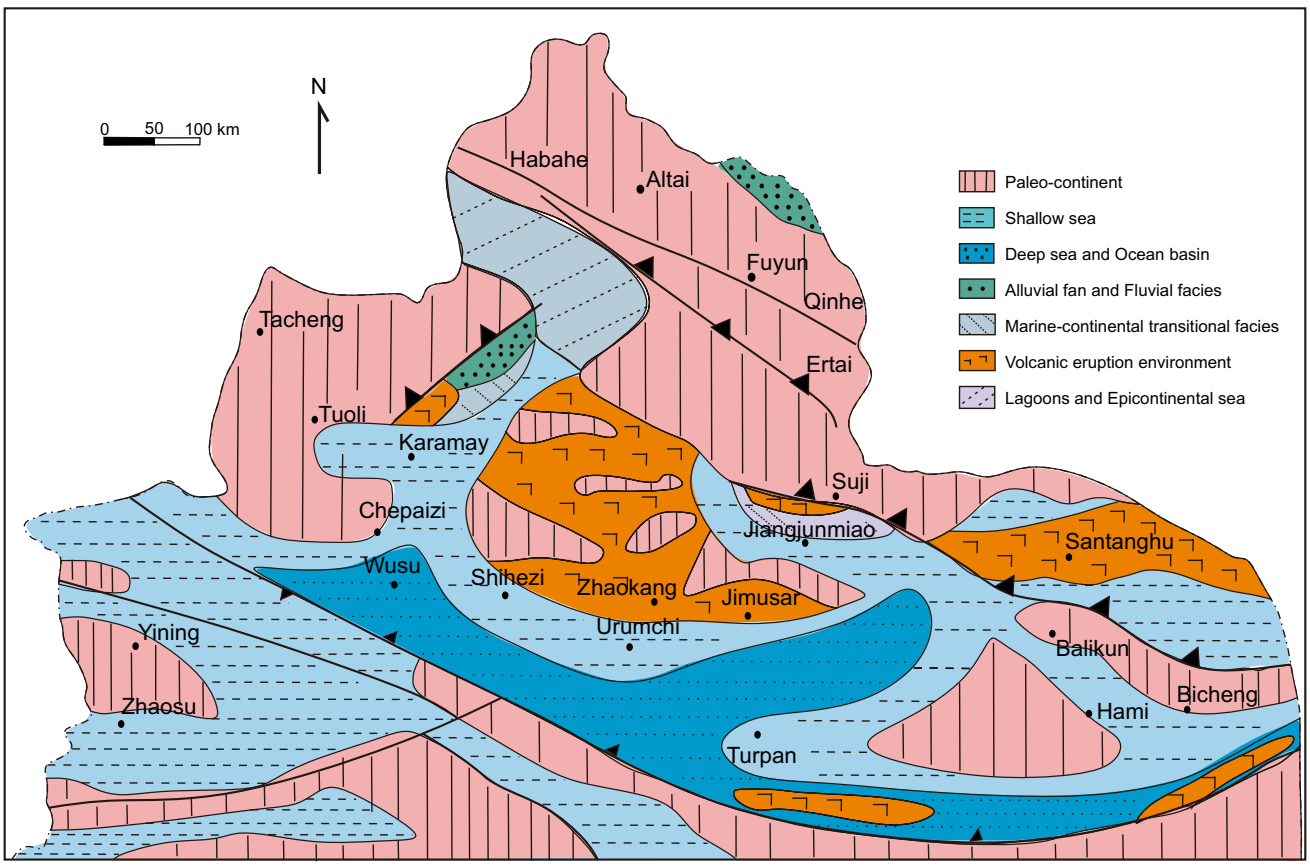

Fig. 1 Lithofacies paleogeography of Late Carboniferous in northeastern part of Xinjiang (from Wu et al. 2008, slightly modified)

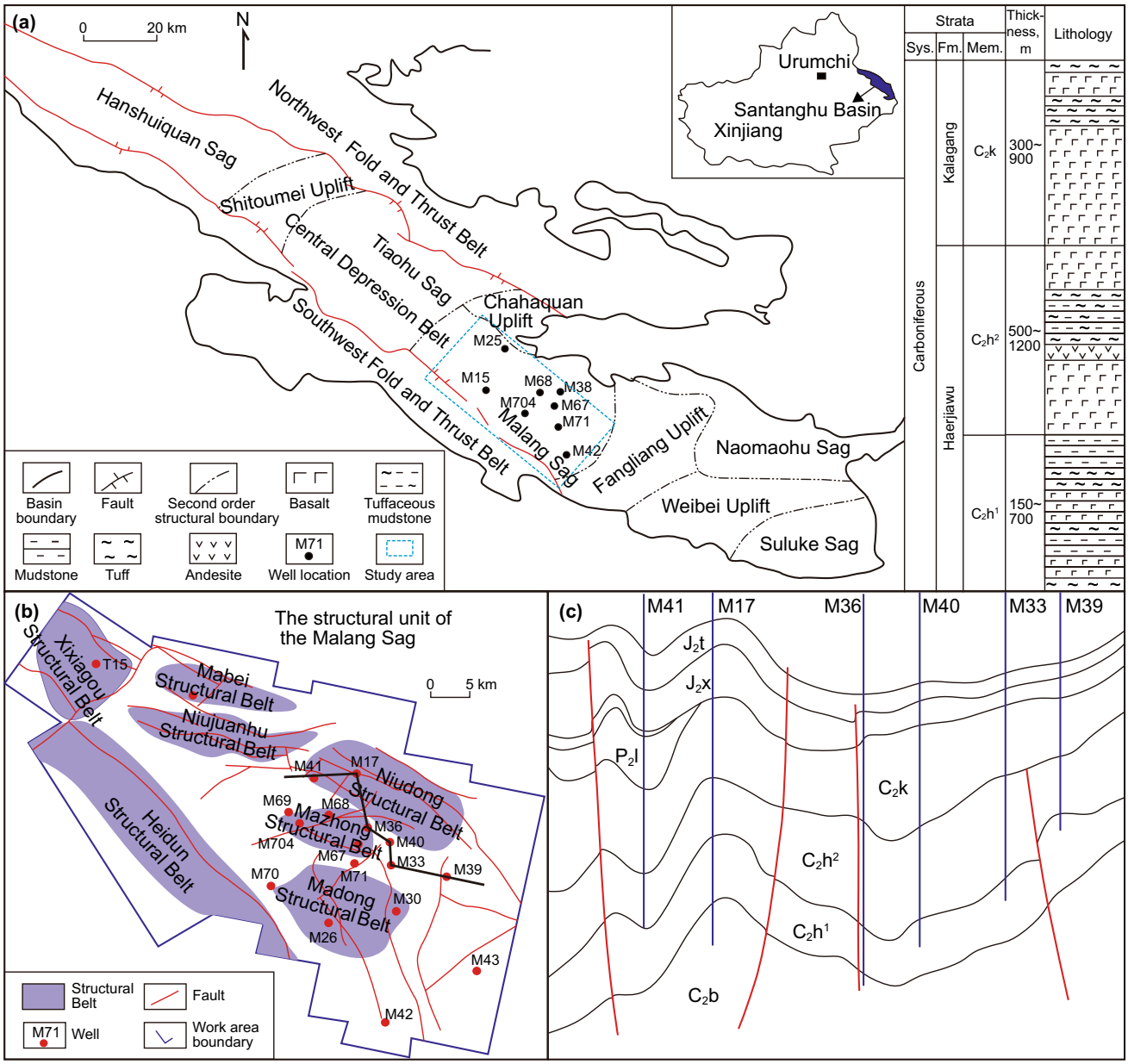

Fig. 2 **a** The location of Malang sag in the Santanghu Basin; **b** Structural unit of the Malang Sag; **c** The stratigraphic profile of Malang sag

3 Samples and analytical methods

3.1 Samples

The samples are mainly collected from the Ha'erjiawu Formation in the Madong structure, Mazhong structure and Niudong structure. The lithology of the samples is mainly carbonaceous mudstone, tuff mudstone and dark gray mudstone. The sampling wells are mainly 11 wells, including M71, M70, M68, M19, M38, M361, M40, M67, M42, M33, ND201, M6704, M6703 and M67. A total of 66 samples were chosen at relatively regular intervals.

3.2 Analytical methods

The above samples were subjected to the whole-rock X-ray diffraction (XRD) (29), scanning electron microscopy with energy-dispersive X-ray spectroscopy (SEM–EDS) (19), thin section identification (19), trace elements (19), saturated hydrocarbon chromatography–mass spectrometry (GC–MS) (19), total organic carbon (TOC) and Rock–Eval pyrolysis (66).

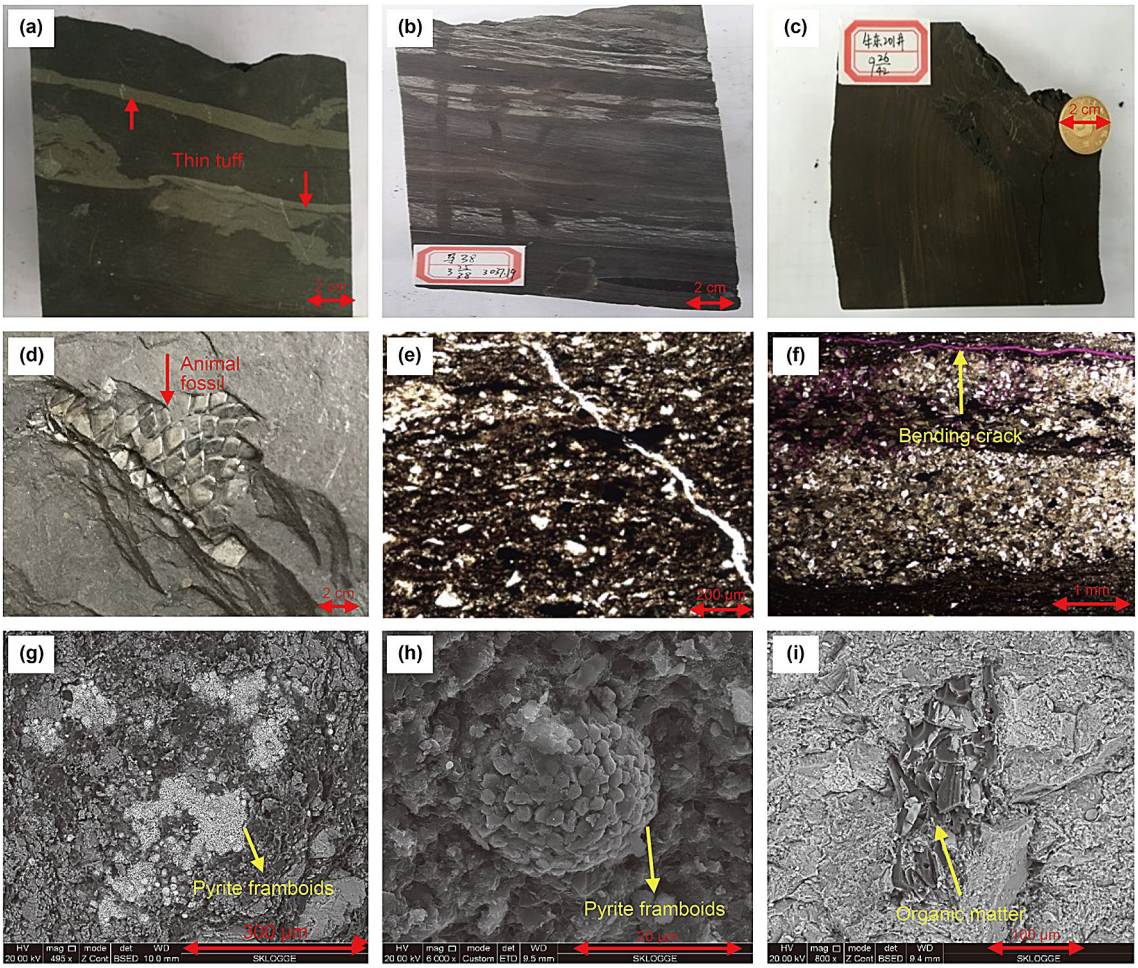

Fig. 3 Characteristics of the organic-rich rocks of the Ha'erjiawu Formation **a** Well M33, 2721.78 m, thin tuff; **b** M38, 3037.19 m, bright tuff lamina; **c** ND 201, 3177.6 m, gray-black, laminated structure; **d** M68, 3653.64 m, fish fossil; **e** M38, 3037.19 m, C_2h, volcanic material and banded organic matter; **f** M68, 3055.05 m, bedding fractures, laminated structure; **g** M38, 3038.2 m, C_2h, pyrite framboids and organic matter; **h** M38, 3038.2 m, pyrite framboids; **i** M361, 3157.4 m, massive organic matter

3.2.1 X-ray diffraction (XRD)

XRD was applied to determine the mineral composition of the samples. The powder samples (≤200 mesh) were analyzed by a Bruker D2 PHASER X-ray diffractometer with Cu-Kα radiation. The testing standard was based on SY/T 5163-2010. The analytical conditions for the XRD were as follows: Cu-Kα radiation, tube voltage with 30 kV, tube current with 10 mA, 0.6 mm emission slit and 8 mm receiving slit, whole-rock random-powder patterns recorded from 4.5° to 50° 2θ. The experiment is conducted at the State Key Laboratory of Petroleum Resource and Prospecting, China University of Petroleum (Beijing).

3.2.2 Microscopic observation

The thin sections observation was carried out on a Leica DM4500P microscope. The SEM observation could recognize minor minerals by electron spectroscopy. In this study, a scanning electron microscope (FEI Quanta 200 F) equipped with an energy-dispersive X-ray spectrometer was used to identify the occurrence of minor minerals in the samples. The testing conditions were as follows: resolution < 1.2 nm, beam voltage 200 V–30 kV, and high vacuum scanning mode. SEM–EDS was conducted at the State Key Laboratory of Oil and Gas Resource and Exploration-Laboratory Completion of Energy Materials Microstructure, China University of Petroleum (Beijing).

3.2.3 Trace elements analysis

As for the trace elements analysis, the powder samples were acid-digested following a two-step digestion (HNO_3–HNO_3: HF: $HClO_4$) method to retain volatile elements in solution. Then, the trace element contents were analyzed by inductively coupled plasma mass spectrometer (ICP-MS) with

Table 1 XRD mineralogy data (unit, wt %)

Well	Depth, m	Clay	Quartz	Calcite	Dolomite	Ankerite	K-feldspar	Plagioclase	Siderite	Pyrite	Anhydrite	Analcime	Laumontite
M42	3987.50	14	41	7	4	0	18	13	0	3	0	0	0
T21	3336.10	25	67	0	0	0	0	8	0	0	0	0	0
T21	3338.20	29	57	0	0	0	0	14	0	0	0	0	0
T11	2941.50	52	31	17	0	0	0	0	0	0	0	0	0
T11	2942.0	55	36	9	0	0	0	0	0	0	0	0	0
T11	2942.50	55	45	0	0	0	0	0	0	0	0	0	0
T11	2944.0	54	42	0	0	0	0	0	1	3	0	0	0
M38	3038.20	15	27	2	0	0	0	47	0	9	0	0	0
M38	3040.50	40	28	9	0	0	0	21	2	0	0	0	0
M38	3041.50	11	30	0	0	0	0	55	1	3	0	0	0
M38	3042.0	44	19	12	2	0	0	21	2	0	0	0	0
M40	2668.50	59	12	5	0	0	0	19	0	5	0	0	0
M40	2732.30	10	14	0	0	0	0	76	0	0	0	0	0
M40	2732.75	8	15	0	0	0	0	76	0	1	0	0	0
M40	2733.0	16	15	0	0	0	0	62	0	7	0	0	0
M68	3655.44	4	64	28	0	0	0	4	0	0	0	0	0
M68	3655.72	22	64	0	0	0	0	10	0	4	0	0	0
M361	3157.40	12	36	0	0	0	0	50	0	2	0	0	0
M361	3158.0	25	34	2	2	0	11	23	0	3	0	0	0
ND201	3176.70	23	40	0	0	0	16	11	0	10	0	0	0
ND201	3177.10	17	65	2	0	0	5	7	2	2	0	0	0
M42	3986.40	0	65	6	3	0	15	11	0	0	0	0	0
M42	3988.30	23	44	5	3	0	13	12	0	0	0	0	0
M42	3987.0	12	70	0	0	0	0	18	0	0	0	0	0
M68	3653.3	13	41	6	0	0	0	31	0	9	0	0	0
M68	3653.88	9	32	20	0	0	0	38	0	1	0	0	0
M361	3156.20	26	29	4	3	0	0	36	2	0	0	0	0
M361	3159.72	12	13	21	0	0	17	31	0	0	0	6	0
M40	2732.04	25	3	3	0	0	0	20	0	0	5	0	44
TC3	3084.0	51	30	2	0	0	0	17	0	0	0	0	0
TC3	3084.50	54	28	2	0	0	0	16	0	0	0	0	0
TC3	3085.0	52	32	2	0	0	0	14	0	0	0	0	0
M71	2837	27	48	3	0	0	0	9	0	7	0	0	0
M71	2928	26	55	3	0	0	0	6	2	2	0	0	0
M71	3142	62	25	4	6	0	0	0	3	0	0	0	0

Table 1 (continued)

Well	Depth, m	Clay	Quartz	Calcite	Dolomite	Ankerite	K-feldspar	Plagioclase	Siderite	Pyrite	Anhydrite	Analcime	Laumontite
M71	3261	31	44	4	0	2	0	12	2	5	0	0	0
M71	3279	44	44	3	0	0	0	8	0	1	0	0	0
M71	3394.8	54	28	4	0	7	0	8	0	0	0	0	0
M71	3400	42	19	3	0	2	0	22	1	0	0	0	11

Perkin Elmer SciexElan 6000 following the criteria of GB/T 14506.30-2010. The experiment was conducted at the Beijing Research Institute of Uranium Geology, China.

3.2.4 Total organic carbon and Rock–Eval pyrolysis

As for the analysis of TOC, the powder samples (< 80 mush) were dealt with diluted HCl to remove the inorganic carbon following Chinese national standard (GB/T 19145-2003). Then, drying samples were analyzed by a LECO CS-230 elemental analyzer. Rock–Eval Pyrolysis was performed on a Rock–Eval OGE-II analyzer. The powder samples were heated at a programmed rate to obtain S_1 (free hydrocarbon), S_2 (pyrolysis hydrocarbon) and T_{max} (the peak temperature of S_2). The experiments are also conducted at State Key Laboratory of Petroleum Resource and Prospecting, China University of Petroleum (Beijing).

3.2.5 Organic geochemistry (biomarker analysis)

The powder samples were extracted with dichloromethane and methanol (97:3, v/v) for 72 h, and then extracted organic matter (EOM) was separated into saturated hydrocarbons, aromatic hydrocarbons, non-hydrocarbon and asphaltene by column chromatography method, and the saturated hydrocarbon was analyzed on GC–MS. GC–MS analysis was performed on an Agilent 7890-5975c gas chromatograph-mass spectrometer with an HP-5MS elastic silica capillary column (60 m × 0.25 mm × 0.25 μm). The gas was boosted at a rate of 1 mL/min. The testing standard was based on GB/T 18606-2001. The experiment is also finished in the State Key Laboratory of Petroleum Resource and Prospecting, China University of Petroleum (Beijing).

4 Results and interpretation

4.1 Mineralogy and lithology

According to the core observations and thin section identification of the organic-rich rocks in the Carboniferous Ha'erjiawu Formation. The organic-rich rocks are mainly dark gray-black with a small number of animal and plant fossils, partially developed horizontal bedding and thin tuff layers (Fig. 3a, b, c, d). Laminated structure, volcanic materials and fractures were observed under a polarized light microscope (Fig. 3e, f). In addition, the scanning electron microscopy (SEM) observations revealed pyrite framboids of various sizes and various forms of organic matter (Fig. 3g, h, i), indicating that the organic-rich rocks of the Ha'erjiawu Formation were deposited in a complex and variable sedimentary environment.

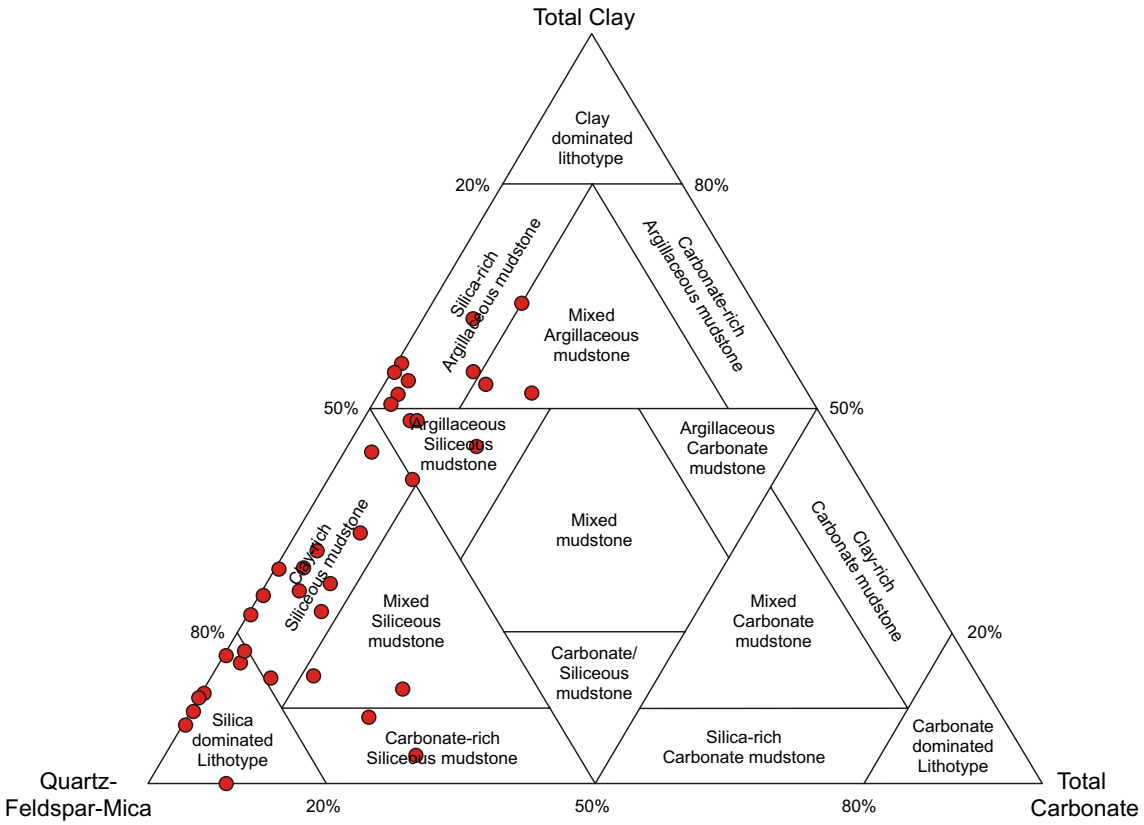

Fig. 4 XRD data plotted on a ternary mineral diagram used to identify mineral facies. The terminology and classification for the shale mineral facies are from Gamero-Diaz et al. (2013)

The X-ray diffraction (XRD) results are presented in Table 1. The organic-rich rocks of the Ha'erjiawu Formation mainly include clay minerals (avg. 29.5%), quartz (avg. 36.7%), feldspar (avg. 23.6%), carbonate (5%) and pyrite (2.9%), and the average content of analcime and laumontite < 2%. The mineralogy-based classification method can be used to effectively discriminate between organic-rich rock types. Based on the XRD data, the ternary mineral diagram classification method proposed by Gamero-Diaz et al. (2013) was used to classify the shale mineral facies. As shown in Fig. 4, the samples mainly plot within five regions, indicating that the organic-rich rocks of the Ha'erjiawu Formation in different wells vary significantly. These sub-classes include silica-dominated mudstone, clay-rich siliceous mudstone, carbonate-rich siliceous mudstone, silica-rich argillaceous mudstone and argillaceous/siliceous mudstone, suggesting that the organic-rich rocks of the Ha'erjiawu Formation are dominated by terrigenous clastic minerals with low carbonate content.

4.2 Trace elements

The composition of trace elements in sedimentary rocks is sensitive to hydrologic changes of environment and can effectively reveal the paleoenvironmental conditions (Morford and Emerson 1999; Liu and Zhou 2007). The analysis results of the trace elements of the samples are shown in Table 2. The concentration coefficients of trace elements in the samples (ratios of element contents in the studied samples versus the upper crust (McLennan 2001) for the samples are illustrated in Fig. 5.

Compared to average values for the upper crust (McLennan 2001), elements V, Sr, Ba, Cu are enriched in most of the samples (Fig. 5). The concentration coefficients of these elements are 0.90–4.88 (avg. 2.48), 0.26–5.15 (avg. 1.35), 0.12–14.91 (avg. 2.52), 0.99–6.52 (avg. 2.78). However, the other trace elements (e.g., Sc, Co, Ni, Rb, Ce) are depleted. The enrichment of certain incompatible elements (V, Sr, Zn, Cu) maybe reflects that the samples received hydrothermal input during deposition (Zhang et al. 2018).

4.3 TOC content and Rock–Eval pyrolysis

The total organic carbon (TOC) and Rock–Eval pyrolysis parameters are important indicators for evaluating the abundance of organic matter in source rocks (Peters 1986). The results of total organic carbon and rock pyrolysis of the samples are shown in Table 3. TOC contents vary from 1.5 to

Table 2 The trace elements contents (ppm) and element ratios of the samples

Sample	M71-1	M71-2	M71-3	M71-4	M71-5	M71-6	M71-7	M70-1	M70-2	M68-1	M68-2	M68-3	M361-1	M361-2	M19-1	M19-2	M38-1	M38-2	M38-3
Depth, m	2837	2975	3225	3261	3394.8	3440	3540	4468	4462	3656	3653.3	3655.85	3158	3157.4	2430.25	2430.46	3038.12	3038.2	3041.38
Li	12.9	21.7	5.06	8.18	29.3	28.7	17	19.9	21.7	20	13.5	17.6	9.52	5.49	7.29	14.03	48.48	23.98	14.22
Sc	6.58	8.02	4.46	7.64	16	12.4	14.9	16.3	17.3	13.6	25	12.2	8.09	7.74	2.09	0.79	54.95	18.88	17.24
V	239	131	247	182	197	156	227	96.5	103	327	522	387	323	467	281	343	343	125	210
Cr	32.3	38.7	16.4	27.4	76	40.4	35.5	123	129	39	125	48	22.1	29.5	16.55	18.53	42.67	94.18	36.69
Co	7.58	7.76	6.33	9.58	15.7	13	13.1	15.3	15.7	15.9	36.4	16.3	10.4	9.93	20.75	13.12	13.2	10.5	15.6
Ni	20.8	20.5	13.5	22.2	38.6	23.7	24.7	40.4	47.1	40	63.7	38.3	18.6	24.1	31.1	41.39	30.09	16.76	40.81
Cu	57.2	37.6	37	59.5	59.9	64.1	24.7	46.3	49	118	163	133	47.2	92.2	/	/	68.05	35.02	98.57
Zn	52.7	43.8	46.9	74.8	97.6	89.4	87.8	98.4	87.2	131	159	111	66.1	95.2	48.35	39.48	91.94	74.29	69.5
Ga	9.69	12.4	6.48	11	22.8	14.1	17	20.4	21.5	19.1	22	111	12.8	9.8	10.57	5.64	10.88	7.67	7.97
Rb	44.5	45.4	25.7	45.9	75.6	26.2	90.4	60.8	65.1	59.7	75.2	59.2	6.88	5.07	141	127	6.9	39.04	5.03
Sr	176	183	138	224	308	381	92	919	893	1803	1094	887	230	215	292	263	205	1161	150
Y	14.8	13.1	9.39	20.2	30.1	29.1	31.8	26.1	26.8	27	23.5	20.5	20.7	15.5	3.02	2.62	92.39	9.74	38.34
Zr	140	120	64.9	125	230	193	209	196	205	260	291	203	134	116	284	249	168	179	182
Nb	8.49	6.13	4.4	8.11	12.7	9.49	9.84	9.02	9.61	18.4	19.8	13.6	7.77	7.27	10.53	7.96	22.26	18.76	15.89
Ba	988	424	2057	2314	734	3551	1479	8200	3176	1380	1649	1026	114	71.4	119	251	79.6	806	69.91
La	19.7	14.7	11	20.2	30.3	28.1	30.4	25.4	25.3	30.7	36.6	28.8	22.6	21	/	/	/	/	/
Hf	3.7	3.73	1.99	3.69	7.39	5.6	6.27	5.89	6.3	8.07	9.5	6.1	3.77	3.24	/	/	/	/	/
Sr/Cu	3.077	4.867	3.730	3.765	5.142	5.944	3.725	19.85	18.22	15.28	6.712	6.669	4.873	2.332	/	/	3.012	33.15	1.522
Rb/Sr	0.253	0.248	0.186	0.205	0.245	0.069	0.983	0.066	0.073	0.033	0.069	0.067	0.030	0.024	0.483	0.483	0.034	0.034	0.034
V/Cr	7.399	3.385	15.06	6.642	2.592	3.861	6.394	0.785	0.798	8.385	4.176	8.063	14.61	15.83	16.98	18.51	8.038	1.327	5.724
Ni/Co	2.744	2.642	2.133	2.317	2.459	1.823	1.885	2.641	3.000	2.516	1.750	2.350	1.788	2.427	1.499	3.155	2.280	1.596	2.616
V/(V+Ni)	0.920	0.865	0.948	0.891	0.836	0.868	0.902	0.705	0.686	0.891	0.891	0.910	0.946	0.951	0.900	0.892	0.919	0.882	0.837
Sr/Ba	0.178	0.432	0.067	0.097	0.420	0.107	0.062	0.112	0.281	1.307	0.663	0.865	2.018	3.011	2.454	1.048	2.575	1.440	2.146
Cu/Zn	1.085	0.858	0.789	0.795	0.614	0.717	0.281	0.471	0.562	0.901	1.025	1.198	0.714	0.968	/	/	0.740	0.471	1.418
Cr/Zr	0.231	0.323	0.253	0.219	0.330	0.209	0.170	0.628	0.629	0.150	0.430	0.236	0.165	0.254	0.058	0.074	0.254	0.526	0.202

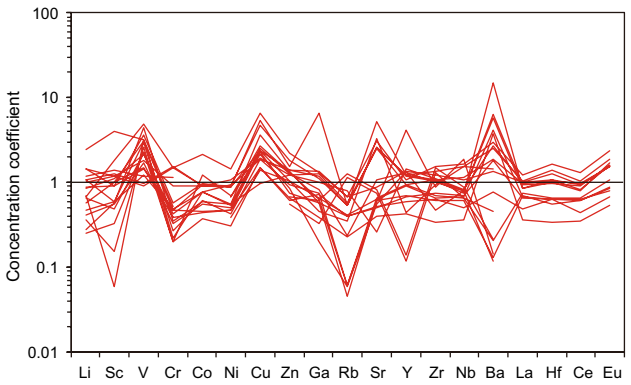

Fig. 5 Concentration coefficients of trace elements, relative to the upper crust (McLennan 2001)

33.62%, with an average of 9.42%, reflecting high organic abundance. S_1 (free hydrocarbons) values range from 0.35 to 16.2 mg HC/g rock, with an average of 3.41 mg HC/g rock, S_2 (pyrolysis hydrocarbon) and hydrocarbon generation potential ($S_1 + S_2$) between 1.5 and 158.6 mg HC/g rock and 1.9–161.10 mg HC/g rock with an average of 27.93 mg HC/g rock and 31.38 mg HC/g rock. Based on the terminology of Peters (1986), the mudstone of the Ha'erjiawu Formation holds good source rock potential (Fig. 6a). The hydrogen index (HI) values are between 32.92 and 737.83 mg HC/g TOC, and the average is 282.21 mg HC/g TOC. This reflects that the source rocks of the Ha'erjiawu Formation have great hydrocarbon generation potential. The T_{max} values are an index for evaluating the maturity of source rocks and mainly vary from 435 to 486 °C, with an average of 447 °C. S_1/TOC values vary between 8.22 and 228.35 mg HC/g TOC, with an average of 40.52 mg HC/g TOC, reflecting that all source rock samples are generally mature with abundant oil content. The cross plot of HI versus T_{max} shows that most of sample points plotted within the kerogen regions of types II_1 and II_2 (Fig. 6b).

4.4 Biomarker compounds

4.4.1 *n*-Alkanes and isoprenoids

The distribution pattern of the *n*-alkanes in the source rocks of the Ha'erjiawu Formation is predominantly bimodal, and the main carbon peaks are at nC_{19}-nC_{23} and nC_{30}-nC_{33} (Fig. 7a). These results are consistent with a mixed source of higher plants and lower aquatic plants (Collister et al. 2007). The acyclic isoprenoids pristane (Pr) and phytane (Ph) were detected in all of the samples (Fig. 7a, Table 4). Pr/Ph ratios of < 1.0 indicate anoxic conditions during early diagenesis, values between 1.0 and 3.0 suggest dysoxic environments, and ratios higher than 3.0 reflect oxic conditions (Didyk et al. 1978; Goossens et al. 1984). However, the Pr/Ph ratio is also affected by maturation (Tissot and Welte 1980). The influence of the different rank on Pr/Ph ratios in the rocks in this study can be ruled out, since no depth-related increase in T_{max} values was observed (Table 3). In the study, the Pr/Ph values mainly range from 1.24 to 2.68, with an average of 1.81 (Table 4). Pr/n-C_{17} values vary from 0.12 to 1.03, with the average of 0.44, Ph/n-C_{18} values range from 0.08 to 0.47, with an average of 0.22 (Table 4).

4.4.2 Steroids and hopanoids

Based on the monitoring mass chromatograms (m/z 217), the distribution of the steranes in all of the samples has similar characteristics. The relative proportions of the C_{29} steranes are highest (21–54%), followed by the C_{28} (22–40%), and the C_{27} steranes (17–37%; Fig. 7c; Table 4).

C_{28} sterols were used as markers for diatomaceous organic matter in Cenozoic sediments (Mackenzie et al. 1982). However, C_{28} sterols have been commonly found in green algae and higher plants (Volkman and Maxwell 1986), and the pronounced increase in the C_{28} sterane content in pre-Cenozoic strata is ascribed to the elevated abundance of diatom and green algae (Jia et al. 2012). C_{27} steranes are typical in zooplankton and red algae, and C_{29} steranes occur in higher plants and some strains of brown and green algae (Huang and Meinschein 1979). As shown in Table 4, the relative proportions of C_{28} steranes of some samples are higher than those of C_{28} steranes, C_{28}/C_{27} ratios range from 0.63 to 2.35, with an average of 1.12. C_{29}/C_{27} ratios range from 0.92 to 2.52, with the average of 1.82, and most of which > 1.5. The predominance of C_{29} steranes in the Ha'erjiawu Formation shale, which was probably derived from sitosterol or stigmasterol (Gomes et al. 2007), is consistent with the dominant origin of organic matter from land higher plants (Canuel et al. 1997). The maturity of the source rocks can be indirectly determined by the 20S/(20S + 20R) isomerization ratio of C_{29} steranes and αββ/(ααα + αββ) isomerization ratio of C_{29} steranes. As shown in Table 4, the average 20S/(20S + 20R) isomerization ratio of C_{29} steranes is 0.42. The average αββ/(ααα + αββ) isomerization ratio of C_{29} steranes was 0.38.

Tricyclic terpanes are derived from bacteria or algae (Simoneit et al. 1990; Peters and Moldowan 1993), which generally have low to moderate contents in the extractable organic matter. As shown in Table 4, tri-/pentacyclic ratios are 0.07–0.52, with an average of 0.18. Generally, in the larger abundance of tricyclic terpanes relative to pentacyclic terpanes (such as hopanes) is related to increasing salinity in water columns (Mello et al. 1988). High contents of gammacerane are generally associated with organic matter deposition in a brackish-saline environment with obvious water stratification (Peters and Moldowan 1993; Schoell

Table 3 TOC and rock pyrolysis data of the samples

Well	Depth, m	TOC, %	S_1, mg HC/g rock	S_2, mg HC/g rock	S_1+S_2, mg HC/g rock	T_{max}, °C	S_1/TOC, mg HC/g TOC	HI, mg HC/g TOC	R_o, %
M19(M19-2)	2430.25	3.51	0.40	1.50	1.90	440.00	11.40	42.74	
M19(M19-1)	2431.46	4.88	0.87	3.27	4.14	437.00	17.83	67.01	
M19	2430.20	5.04	1.61	6.03	7.64	430.00	31.94	119.64	
M19	2430.90	6.06	1.64	11.15	12.79	430.00	27.06	183.99	
M19	2431.40	6.39	4.37	11.05	15.42	425.00	68.39	172.93	
M38(M38-1)	3038.12	13.4	6.84	34.89	42.4	442	51.04	327.3	0.70
M38(M38-2)	3038.20	19.20	2.52	93.42	95.94	445.00	13.13	486.56	
M38	3040.50	10.30	1.22	6.14	7.36	449.00	11.84	59.61	
M38(M38-3)	3041.38	12.10	3.85	53.79	57.64	439.00	31.82	444.55	
M38(M38-5)	3042.24	8.58	5.17	19.73	24.9	438	60.26	229.93	0.73
M38	3379.00	5.68	2.52	24.13	26.65	447.00	44.37	424.82	
M38	3381.00	4.19	2.15	18.75	20.90	450.00	51.31	447.49	
M38	3382.00	4.84	1.73	18.01	19.74	447.00	35.74	372.11	
M38	3383.00	4.40	1.52	18.80	20.32	445.00	34.55	427.27	
M38	3384.00	3.32	1.51	9.91	11.42	446.00	45.48	298.49	
M38	3385.00	5.91	2.49	21.88	24.37	447.00	42.13	370.22	
M38	3388.00	4.09	1.57	12.06	13.63	448.00	38.39	294.87	
M38	3389.00	4.24	2.14	13.46	15.60	448.00	50.47	317.45	0.73
M67(M67-2)	3225.00	11.28	9.20	15.68	24.94	443.00	81.56	139.01	
M67(M67-1)	3219.00	6.02	3.13	5.97	9.22	440.00	51.99	51.99	
M67(M67-3)	3301.00	10.3	2.55	15.88	18.44	443.00	24.76	325.41	
M6703(M6703-1)	3264.00	7.53	2.49	16.31	18.80	440.00	33.07	216.60	
M40	2668.50	4.49	0.64	14.87	15.51	436.00	14.25	331.18	
M40	2732.30	6.76	2.60	20.28	22.88	440.00	38.46	300.00	
M40	2732.75	7.24	5.83	29.60	35.43	445.00	80.52	408.84	
M40	2733.00	13.20	9.51	56.94	66.45	436.00	72.05	431.36	
M68(M68-2)	3653.30	21.10	8.53	28.59	37.12	451.00	40.43	135.50	
M68	3655.72	8.90	1.55	2.93	4.48	482.00	17.42	32.92	
M68(M68-1)	3656.0	8.95	1.88	4.29	6.17	484	21.01	47.94	
M68	3472.8	3.55	1.11	12.43	13.54	446	31.27	350.14	
M68	3497.2	6.77	2.94	23.64	26.58	447	43.43	349.19	
M68	3546	3.89	0.7	2.88	3.58	447	17.99	74.04	
M68	3549.2	10.1	6.58	41.49	48.07	450	65.15	410.79	0.90
M68	3554.1	1.94	4.43	8.76	13.19	437	228.35	451.55	
M68	3557	13.53	5.52	57	62.52	449	40.80	421.29	
M68	3564	12.21	4.94	43.27	48.21	446	40.46	354.38	
M68	3640.4	6.86	2.34	23	25.34	443	34.11	335.28	
M68	3646.9	10.5	1.57	37.91	39.48	446	14.95	361.05	
M68(M68-3)	3655.85	9.22	1.14	3.31	4.45	486	12.36	35.91	
M33	2721.54	9.83	1.33	30.36	31.81	443	13.53	405.34	
M361(M361-2)	3157.40	26.50	16.20	98.51	114.71	449	61.13	371.74	
M361(M361-1)	3158.00	22.20	16.10	114.49	130.59	447	72.52	515.72	0.63
M361(M361-3)	3156.20	1.50	0.35	2.90	3.25	450	23.33	193.33	
M361(M361-4)	3159.72	5.07	3.91	16.47	20.42	442	77.12	324.85	
ND201	3176.70	24.60	2.37	158.60	161.10	447	9.63	644.72	0.72
ND201	3177.10	14.60	1.20	7.92	9.49	447	8.22	54.25	
M42	3987.50	11.4	1.69	6.77	8.53	478	14.82	90.69	
M42	3986.40	4.49	3.22	4.06	7.93	465	71.71	108.85	

Table 3 (continued)

Well	Depth, m	TOC, %	S_1, mg HC/g rock	S_2, mg HC/g rock	S_1+S_2, mg HC/g rock	T_{max}, °C	S_1/TOC, mg HC/g TOC	HI, mg HC/g TOC	R_o, %
M42	3988.30	2.83	0.92	2.42	3.62	472	32.51	114.69	1.62
M42	3987.0	8.0	1.45	5.17	6.69	470	18.13	99.23	
M70(M70-2)	4462.0	6.06	1.62	5.32	6.94	463	26.73	87.75	
M70(M70-1)	4468.0	6.69	3.41	7.55	10.96	465	50.97	50.94	
M71(M71-8)	2785	4.95	6.57	36.53	43.1	437	132.73	737.83	
M71(M71-9)	2786.5	3.01	1.72	22.03	23.75	442	57.14	731.41	
M71(M71-1)	2837.00	19.80	10.09	110.44	120.53	439	50.96	557.78	
M71(M71-2)	2975.00	9.42	2.12	28.85	30.97	437	22.51	306.17	
M71	3142.00	5.97	3.15	10.65	13.80	439	52.76	178.33	
M71(M71-3)	3225.0	33.62	5.95	87.34	93.29	443	17.70	259.79	0.73
M71(M71-4)	3261.00	26.79	4.5	74.15	78.65	445	16.80	276.78	
M71	3279.00	12.63	2.74	49.37	52.11	444	21.69	390.89	
M71(M71-5)	3394.80	6.03	1.31	21.21	22.52	444	21.72	351.68	
M71	3584.00	8.826	2.19	10.72	12.91	441	24.81	121.46	0.82
M71(M71-7)	3540.00	6.805	1.83	18.12	19.95	445	26.89	266.27	
M71	3315.00	18.52	1.74	6.61	8.35	446	9.40	35.69	0.76
M71(M71-6)	3440.00	12.37	2.10	53.34	55.44	448	16.98	431.20	
M71	3400.00	3.84	1.94	10.25	12.19	441	50.52	266.86	

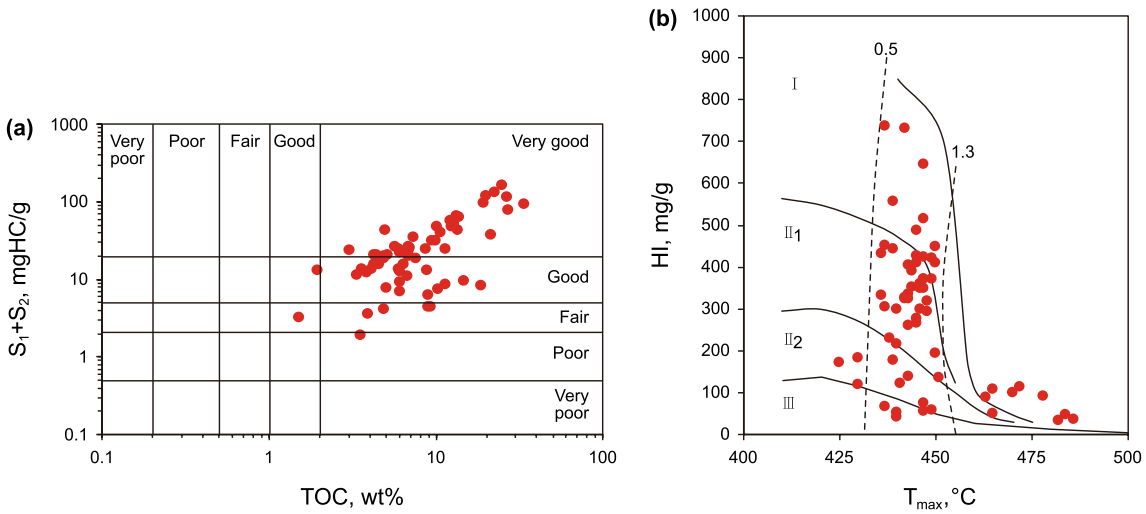

Fig. 6 Plot of the Rock–Eval pyrolysis parameters for the samples. **a** Plot of (S_1+S_2) versus total organic carbon (TOC); **b** Plot of HI versus T_{max} [according to Espitalié et al. (1984)]

et al. 1994). As shown in Table 4 and Fig. 7b, the gammacerane indexes vary between 0.01 and 0.35, with an average of 0.08. There is a slightly positive correlation between gammacerane index and the tricyclic terpanes/pentacyclic terpanes ratio (Fig. 8).

5 Discussion

5.1 Thermal maturity and organic matter source

The vitrinite reflectance (R_o) values mainly range from 0.63 to 0.90%, indicating that the organic matter is mature (Table 3). T_{max} measured values (420–480 °C, average of 449 °C) also support oil window maturity, but a small

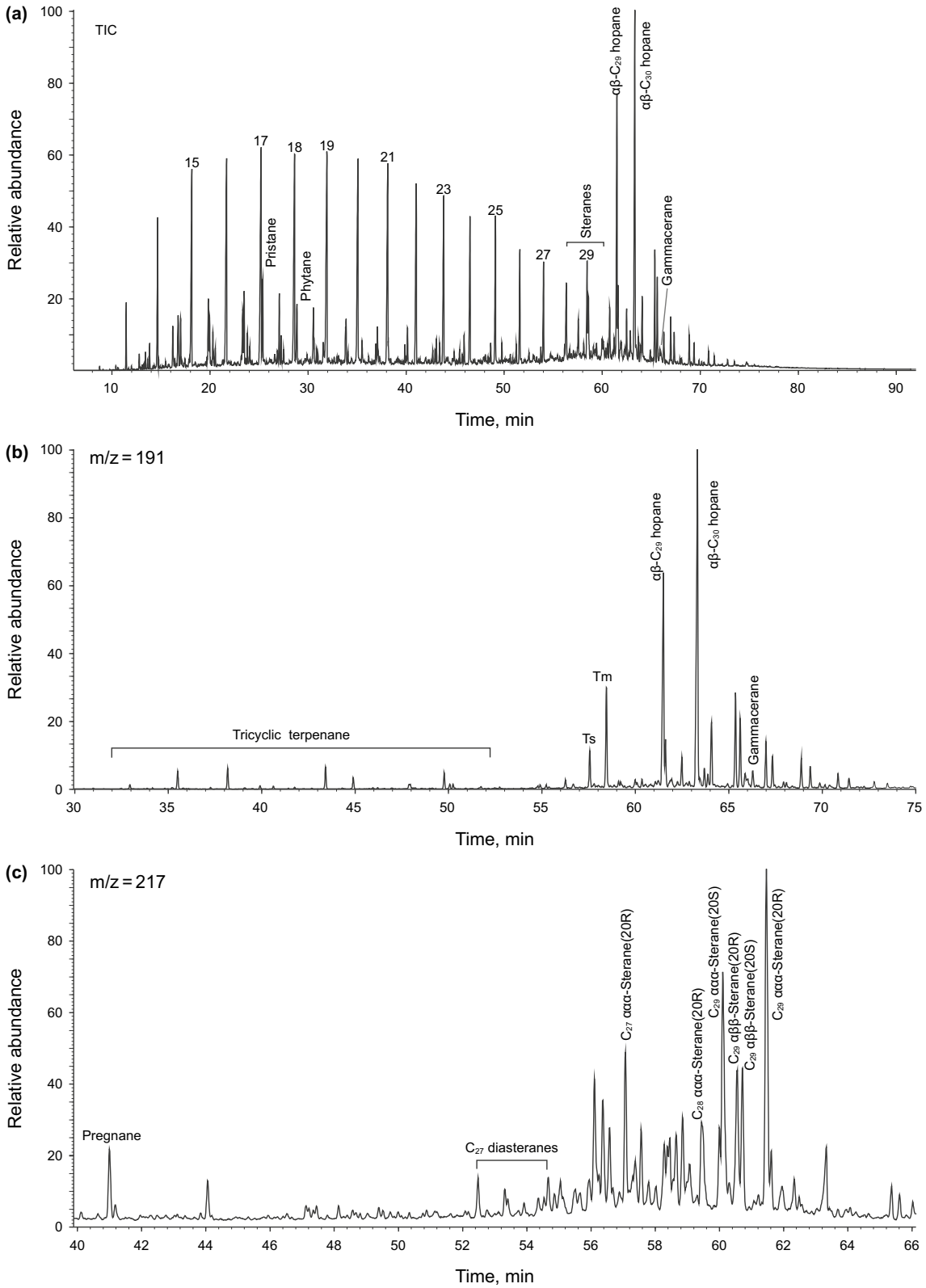

Fig. 7 **a** M38-2, gas chromatograms (total ion current) of the saturated hydrocarbon fractions; **b** M38-2, mass chromatograms (m/z = 191) of the hopane; **c** M38-2, mass chromatograms (m/z = 217) of the steranes and diasteranes

Table 4 Concentration ratios of biomarker components from the Ha'erjiawu Formation

Sample	Depth, m	Pr/nC_{17}	Ph/nC_{18}	Pr/Ph	C_{27} steranes	C_{28} steranes	C_{29} steranes	C_{29}/C_{27} steranes	20S/(S + R) C_{29}steranes	αββ/(ααα + αββ) C_{29}steranes	Tri-/pentacyclic	Gammacerane index
M38-2	3038.20	0.42	0.21	2.20	22	24	54	2.47	0.43	0.34	0.09	0.05
M38-4	3040.50	0.69	0.41	1.71	23	23	54	2.37	0.46	0.38	0.09	0.05
M38-5	3042.24	0.38	0.18	1.48	34	22	44	1.32	0.38	0.40	0.06	0.02
M38	3037.16	0.57	0.34	1.56	24	26	50	2.07	0.45	0.49	0.07	0.04
M40-1	2732.75	1.03	0.47	2.07	25	25	50	2.04	0.45	0.32	0.07	0.06
M42-1	3987.5	0.14	0.09	1.68	33	32	35	1.06	0.50	0.40	0.36	0.13
M361-3	3156.2	0.39	0.21	1.87	23	33	44	1.94	0.47	0.39	0.12	0.04
M361-4	3159.72	0.76	0.35	2.07	28	27	45	1.61	0.52	0.48	0.11	0.03
M71-8	2785	0.64	0.27	1.47	30	27	43	1.42	0.42	0.37	0.12	0.06
M71-9	2786.5	0.63	0.29	1.24	31	26	43	1.40	0.42	0.36	0.12	0.06
M71-1	2837	0.36	0.15	2.68	31	24	45	1.47	0.37	0.31	0.13	0.05
M71-2	2975	0.92	0.39	2.34	29	24	47	1.63	0.34	0.33	0.11	0.04
M71-3	3225	0.12	0.08	1.47	22	27	51	2.32	0.32	0.42	0.07	0.01
M71-4	3261	0.15	0.09	1.52	25	25	50	2.00	0.36	0.39	0.12	0.03
M71-7	3540	0.14	0.10	1.27	37	29	34	0.92	0.31	0.41	0.50	0.13
M68-1	3653.30	0.21	0.14	1.43	28	32	40	1.41	0.35	0.33	0.52	0.30
M68-2	3655.85	0.18	0.12	1.76	17	40	43	2.52	0.39	0.28	0.42	0.35
M6703-1	3264	0.39	0.18	2.15	24	28	48	2.02	0.47	0.40	0.12	0.06
M67-1	3219	0.37	0.18	1.95	22	31	47	2.14	0.49	0.42	0.13	0.03
M67-2	3225	0.36	0.17	2.07	22	30	48	2.18	0.48	0.43	0.12	0.04
M67-3	3301	0.37	0.19	2.04	20	33	47	2.37	0.47	0.38	0.12	0.05

Tri-/pentacyclic: tricyclic terpanes/pentacyclic terpanes

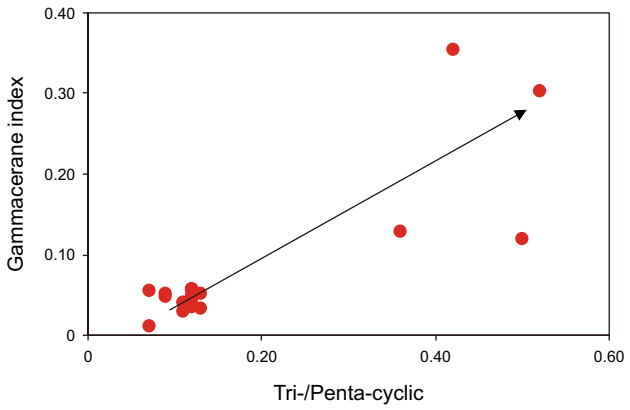

Fig. 8 Cross-correlation of the gammacerane index (GI: gammacerane/C_{30} 17α(H),21β(H)-hopane versus tricyclic terpanes/pentacyclic terpanes (tri-/pentacyclic)

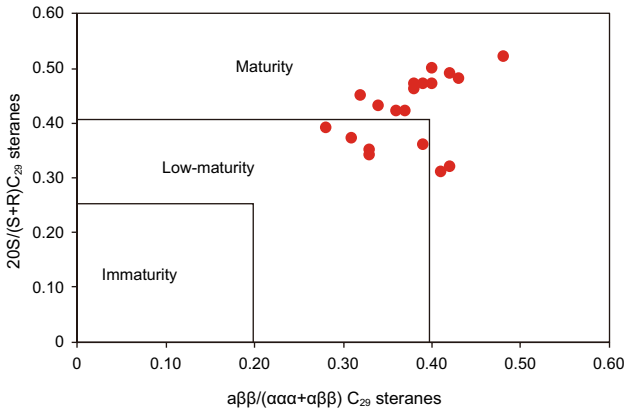

Fig. 9 Plot of 20S/(S + R) C_{29} steranes versus αββ/(ααα + αββ) C_{29}

amount of data falls within the zone of high-maturity ($T_{max} > 460$ °C, $R_o > 1.3\%$; such as the sample of M42, 3988.30 m). These abnormal T_{max} values may be ascribed to the intrusion of igneous rocks into the source rocks (Zhang et al. 2006a). Furthermore, the oil window maturity is confirmed by the C_{29} ααα 20S/(20S +20R) and C_{29} αββ/(αββ +ααα) sterane values, most of which fall within the maturity zone (Fig. 9). In summary, the data indicate that the Ha'erjiawu Formation has reached the mature stage, consistent with the data provided by Wang et al. (2013a, b).

The Pr/*n*-C_{17} and Ph/*n*-C_{18} ratios also indicate mixed organic matter deposited in a dysoxic environment (Fig. 12b). The distribution pattern of the carbon numbers for ααα 20R steranes ($C_{29} > C_{27} > C_{28}$) indicates a mixed contribution of plankton/algal and terrigenous organic matter. The result is supported by the C_{27}–C_{28}–C_{29} regular sterane ternary plot (Fig. 10), and the high C_{28}/C_{27} regular sterane ratios of some samples indicate diatoms and dinoflagellates mainly contribute to the C_{28} sterane. This is consistent with the interpretation on high content of C_{28} steranes from the tuffaceous mudstone of the Permian source rocks in the Junggar Basin (Liu et al. 2017).

5.2 Paleoenvironmental conditions

Redox conditions of a water column are important indicators for investigating sedimentary environments. Previous studies have shown that some geochemical indicators, such as V/Cr, Ni/Co, V/(V + Ni), and Pr/Ph, are useful indicators of the water redox conditions (Hatch and Leventhal 1992; Jones and Manning 1994; Song et al. 2017). Jones and Manning (1994) suggested that V/Cr ratios of < 2, 2–4.25, and > 4.25 correspond to oxic, dysoxic, and suboxic to anoxic conditions, respectively. They also suggested that Ni/Co ratios of < 5, 5–7, and > 7 correspond to oxic, dysoxic, and anoxic conditions, respectively. According to Hatch and Leventhal (1992), V/(V + Ni) ratios of 0.46–0.60 reflect dysoxic conditions, ratios of 0.54–0.82 reflect anoxic conditions, and ratios of > 0.84 represent euxinic conditions. The source rock samples analyzed in this study have V/Cr ratios ranging from 0.78 to 18.5, with an average of 9.23, and V/(V + Ni) ratios ranging from 0.69 to 0.95, with an average of 0.88 (Table 2, Fig. 11a), which consistently suggests dysoxic-anoxic sedimentary environments for the Ha'erjiawu Formation. The Pr/Ph ratios range from 1.2 to 2.7, with an average of 1.8. More than 58% of the samples have Pr/Ph ratios of 1–2 (Fig. 12a), suggesting dysoxic conditions. In addition, the Pr/*n*C_{17} versus Ph/*n*C_{18} plot further suggests a mixed organic matter source and weak oxidizing conditions (Fig. 12b). However, the Ni/Co ratios are < 5.0, with an average of 2.04 (Fig. 11b), suggesting an oxic depositional environment, which is contrary to the development of the thick, high rganic matter abundance dark mudstone and pyrite framboids in the Ha'erjiawu Formation (Fig. 3g–h). It is generally believed that in the anoxic-euxinic environment, the growth rate of pyrite framboids is slower that of pyrite in a dysoxic-oxic conditions (Wang et al. 2013a). Due to the influence of a reducing environment and hydrodynamic conditions, authigenic pyrite has a large average diameter with a wide range of variations (Gallego-Torres et al. 2015; Wilkin et al. 1996). As shown in Fig. 3, the Ha'erjiawu Formation includes large-scale pyrite framboids (> 20 μm, Fig. 3g). In addition, we also found small-scale pyrite framboids (< 10 μm, Fig. 3h), which are associated with organic matter. This also indirectly indicates that the water column was not always anoxic-euxinic conditions during the deposition of the Ha'erjiawu Formation. Thus, the water column may have had low oxygen content and varying redox conditions. In general, the Ni/Co ratio is susceptible to diagenesis and should not be used as a reliable indicator (Zhang et al. 2018). Therefore, when using element geochemical indicators to

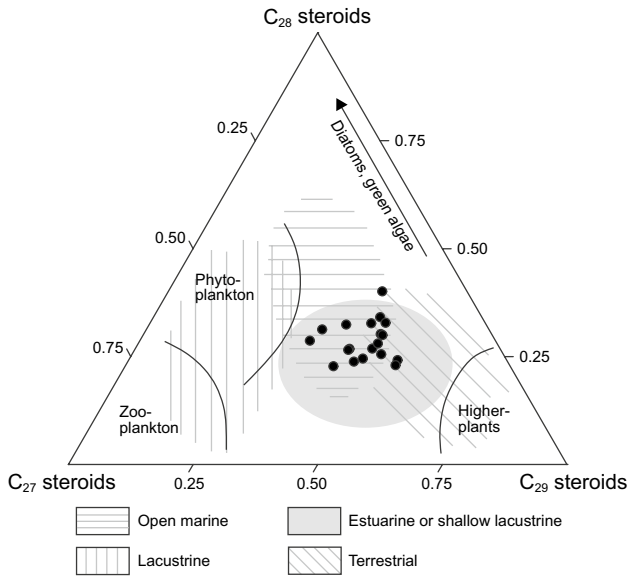

Fig. 10 Ternary plot of the relative proportions of C_{27}, C_{28}, C_{29} steranes (according to Farhaduzzaman et al. 2012)

determine the redox conditions, the applicability and influencing factors should be considered and should be combined with the organic geochemistry, petrology and mineralogy to comprehensively determine the redox conditions of the water column. In addition, during the deposition of the Ha'erjiawu Formation, the inorganic geochemical indexes (V/Cr and V/(V + Ni)) indicate dysoxic-anoxic conditions, whereas organic geochemical indicators, petrology, and mineralogy indicate dysoxic environments. These contradictions may be related to the volcanic eruption and hydrothermal activity, which lead to the enrichment of certain incompatible elements near volcanic edifice and also caused the high V/(V + Ni) ratios (Jin and Zhai 2003; Jin et al. 2006). During the volcanic intermission, volcanic ash and hydrothermal fluids can stimulate algal/bacterial growth by releasing nutrients and transition metals to into waters, which can consume a lot of oxygen in the water, causing intermittent anoxic conditions (Wang et al. 2013b). This is also conductive to the preservation of organic matter. However, during the volcanic eruption, magma and pyroclastic rocks frequently fall into the water column around the volcanic edifice. As a result, the water column is frequently disturbed, and the redox conditions may be dysoxic-oxic (Wang et al. 2013b). Moreover, the water column far away from the volcanic edifice may be dysoxic-anoxic. Therefore, the redox conditions of the Ha'erjiawu Formation are very complicated and were significantly influenced by the volcanic and hydrothermal activity. All of the above indicators suggest episodic transitions between dysoxic and anoxic depositional environments, but a predominantly dysoxic environment.

The salinity of the water column in a lacustrine basin has an important effect on the biological processes and mineral formation. The water salinity can be characterized by the B content and other geochemical indicators, such as Sr/Ba, Rb/K and B/Ga ratios (Campbell 1965; Banerjee and Goodarzi 1990; Ye et al. 2016; Li and Chen 2003). Although

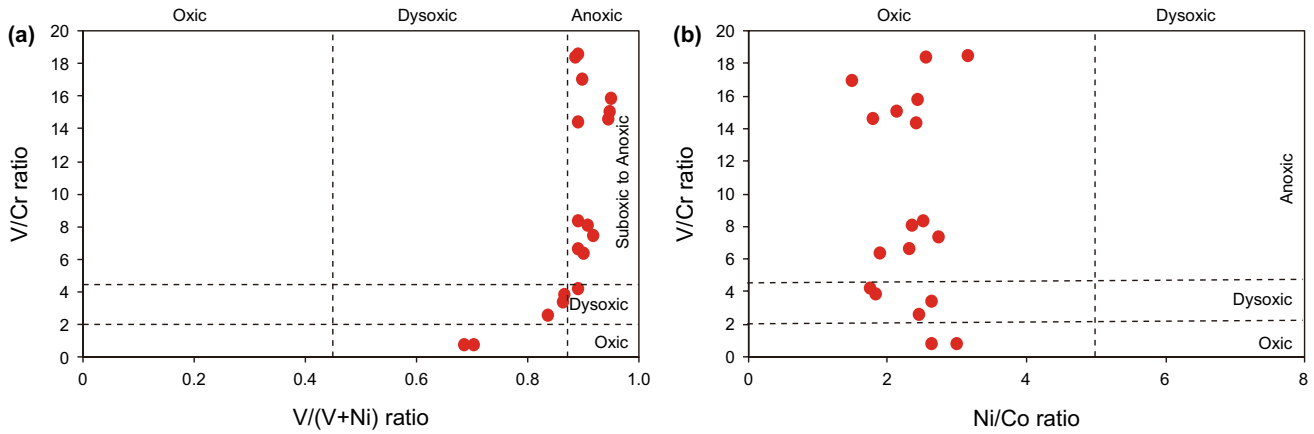

Fig. 11 Plots of the paleoenvironment proxies, indicating the redox condition of the samples; **a** V/Cr versus V/(V + Ni); **b** V/Cr versus Ni/Co

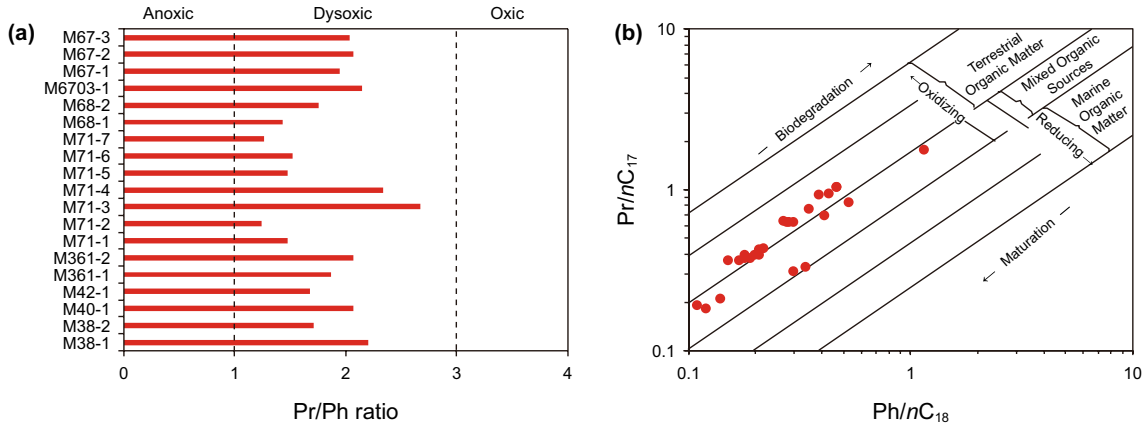

Fig. 12 **a** Pr/Ph distribution diagram; **b** Cross plot of Pr/n-C_{17} versus Ph/n-C_{18}

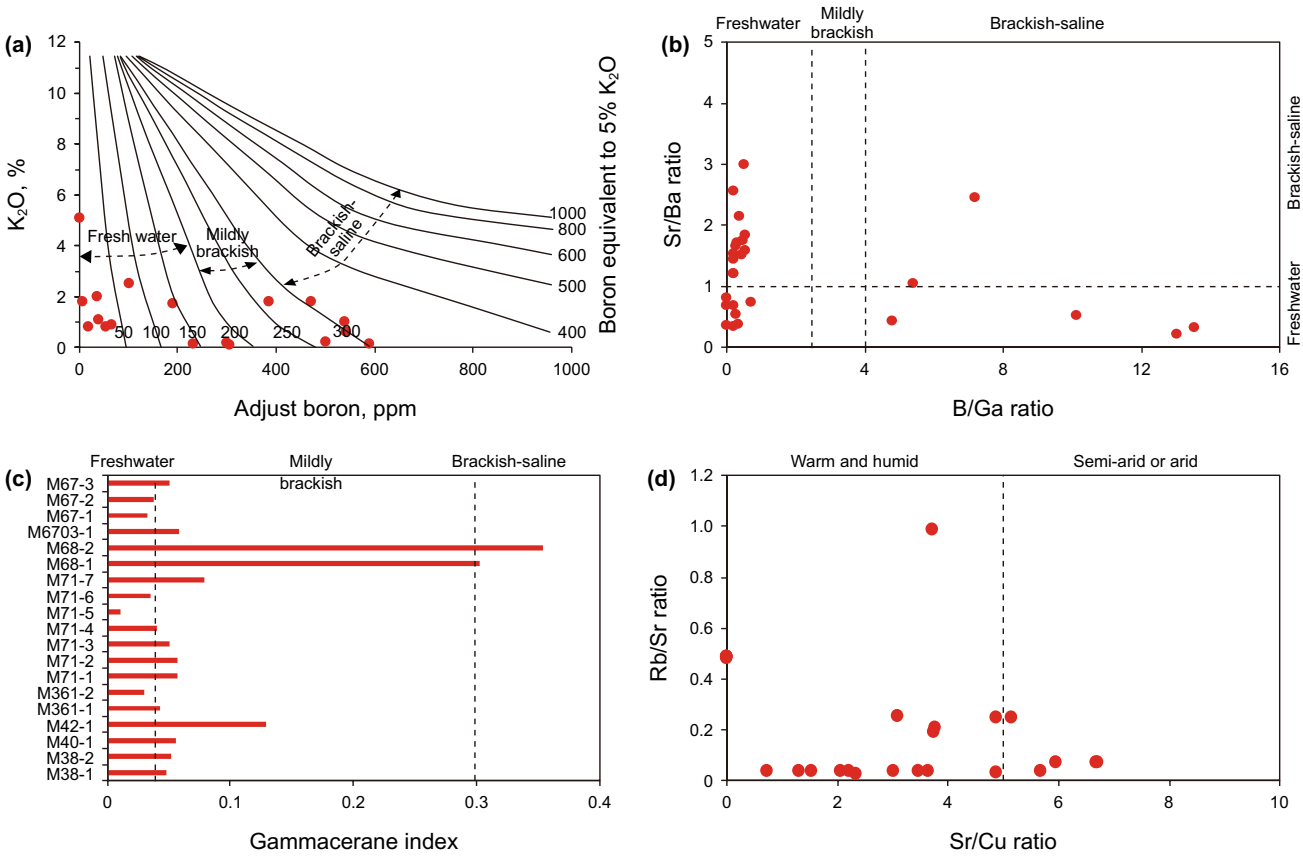

Fig. 13 Discriminant plots of paleosalinity and paleoclimate. **a** plot of K_2O versus adjust B content, **b** plot of Sr/Ba versus B/Ga; **c** gammacerane index distribution diagram, and **d** plot of Sr/Cu versus Rb/Sr

there is still a controversy concerning the source of the B in sedimentary rocks, most scholars suggest that the B content has a good positive correlation with the sedimentary water salinity. Banerjee and Goodarzi (1990) believed that B contents of < 50 ppm reflect freshwater, values of 50–110 ppm reflect mildly brackish water, and values of > 110 ppm correspond to brackish-saline environment. Previous studies have shown that the mudstone has a high B content, and the illite has a strong B adsorption capacity element compared with those of other clay minerals. Thus, the boron content should be combined with clay mineral analysis to objectively determine the sedimentary environment. Walker et al. (1963)

proposed the conversion 8.5% of the K content of the illite into the adjusted boron mass fraction of the illite and that the B content of illite is related to the K mass fraction. In order to allow for comparative analysis under the same conditions, it is necessary to calculate the B mass fraction equivalent to 5% K_2O, which is called the equivalent boron mass fraction. According to the theoretical conversion curve published by Walker et al. (1963), the equivalent B contents were obtained using the graphical method (Fig. 13a). Equivalent B contents of > 300 ppm, 200–300 ppm and < 200 ppm represent brackish-saline, mildly brackish, and freshwater environment, respectively (Walker et al. 1963; Liu et al. 2011). The analysis results of the samples show that (part of the data is from Liu et al. 2011) the equivalent B content of the source rocks of the Ha'erjiawu Formation ranges from 7 ppm to 310 ppm, with most being 300 ppm, reflecting freshwater-mildly brackish sedimentary environment (Fig. 13a).

The B/Ga ratio can also be used to determine the salinity of the water column. Generally speaking, B/Ga ratios of > 4, 2.5–4.0, < 2.5 represent brackish-saline, mildly brackish and freshwater environments, respectively (Campbell 1965). The Sr/Ba ratio also increases with increasing salinity. In general, for the clays or mudstones, the Sr/Ba ratios of freshwater sediments are < 1, and the Sr/Ba ratios of seawater or saline water are > 1. In addition, the Sr/Ba ratio sharply increases in the transitional environment between freshwater and marine. The gammacerane index and the tricyclic terpane index (Tri-/pentacyclic ratio) of biomarker compounds can also reflect the salinity of the water column (Fig. 8). It is generally believed that gammacerane indexes of 0.08–0.3 correspond to freshwater-mildly brackish environments (Zhang et al. 2000; Zou et al. 2009; Song et al. 2017). The analysis results show (Fig. 13b, c, and Table 5) that the B, B/Ga, Sr/Ba and gammacerane indexes (salinity indicators) are 1.57–99.83 with an average of 30.98; 0.06–3.01 with an average of 0.93; 0.12–10.11 with an average of 3.1; and 0.01–0.35 with an average of 0.08, respectively. All the above four salinity indicators consistently suggest that the Ha'erjiawu Formation was deposited in a freshwater-mildly brackish environment, with local areas brackish-saline water. In addition, the plot of gammacerane index versus Tri-/pentacyclic ratio supports this view (Fig. 8). The main reason for this environment is that the Ha'erjiawu Formation was deposited between the closing of the ocean basin in the Early Carboniferous and the intracontinental extensional tectonics of the post-collision environment in the Early Permian. There may have been residual intercontinental seas locally (Lin et al. 1997; Wu et al. 2008), in which the salinity of the water column is high.

In general, the salinity of the water column is closely related to the evaporation in arid or semiarid climates. Under warm and humid climatic settings, strong rainfall and provenance supply lead to a low salinity water column. Evaporation in an arid or semiarid climate causes the salinity to increase sharply (Zhang et al. 2018). Previous studies have shown that the Sr/Cu and Rb/Sr ratios can be used to

Table 5 Trace element concentrations and adjust B concentrations of the Ha'erjiawu Formation mudstone (some data from Liu et al. 2011)

Well	Depth, m	Sr, ppm	Ba, ppm	B, ppm	Ga, ppm	K_2O, %	Adjust boron, μg/g
M39	1687.3	341	284	3.16	8.3	1.6	16.79
M33	1523.1	639	513	63.33	6.3	1.0	538.31
M29	2185.7	292	314	8.56	6.9	2.0	36.38
M38	3040.8	868	641	38.08	12.7	1.7	190.40
M38	3039.4	1161	806	1.78	7.2	1.8	8.41
M40	2668.6	171	227	7.15	10.3	0.9	67.53
M40	2732.8	119	258	1.85	15.6	0.8	19.66
M43	1546	476	366	5.03	11.3	0.8	53.44
M45	2484.4	230	414	1.57	6.6	5.1	2.62
M45	3205	373	706	81.51	21.5	1.8	384.91
T16	3206.6	165	631	99.83	25.8	1.8	471.42
T16	3286.9	99	168	11.79	15.7	0.2	501.08
M42	3988.2	269	765	30.25	7.3	2.5	102.85
M43	1545.9	476	366	5.03	11.3	1.1	38.87
T11	2942.8	14	49	38.31	20.7	0.6	542.73
M19	2430.27	292	119	75.86	10.57	0.09	590.02
M19	2430.87	115	258	29.71	6.23	0.09	231.08
M19	2431.07	263	251	30.48	5.64	0.07	304.80
M19	2431.3	91.03	171	55.4	5.48	0.13	298.31

estimate paleoclimate conditions (Fan et al. 2012). Generally, Sr/Cu ratios of 1–5 indicate warm and humid climatic conditions, whereas ratios of > 5 correspond to arid climatic conditions. The high Rb/Sr ratios usually represent warm and humid climatic conditions. In this study, the climatic indicators show that most of the samples have Sr/Cu ratios of < 5, and the Rb/Sr ratios vary between 0.02 and 0.98, with an average of 0.2. The Ha'erjiawu Formation was mainly deposited in a warm and humid climate, and there may have been intermittent arid climatic conditions (Fig. 13d). In addition, the fish fossils found in the Carboniferous source rocks also support these paleoclimate conditions (Fig. 2d), and these fossils are similar to palaeonisciformes found in the Permian Lucaogou Formation organic-rich rocks in Santanghu Basin. Furthermore, recent work by Liu et al. (2015) and Zhang et al. (2018) have demonstrated that the Lucaogou Formation was deposited in a warm and humid climatic setting through paleobotany and palaeonisciformes studies.

Based on the above analysis, the organic-rich mudstone of the Late Carboniferous Ha'erjiawu Formation in the Santanghu Basin was deposited in a warm and humid, freshwater-mildly brackish water environment. The redox conditions of the Ha'erjiawu Formation were very complicated and were significantly influenced by volcanic and hydrothermal activity. This suggests an episodic transition between dysoxic and anoxic depositional environments, with a predominantly dysoxic environment.

5.3 Controls on organic matter enrichment

Organic matter enrichment is a complicated, nonlinear geological process controlled by the interaction of multiple factors (Liu et al. 2017; Zhang et al. 2018). In general, anoxic-euxinic and brackish-saline water columns are conducive to the enrichment and preservation of organic matter, and source rocks formed in these environments have high organic matter abundances. The above discussion has demonstrated that the Ha'erjiawu Formation was deposited in a dysoxic, freshwater-mildly brackish environment. Moreover, frequent volcanic activity resulted in the frequent disturbance of the water column near the volcanic edifice. However, in such a sedimentary environment, the Ha'erjiawu Formation shales still developed source rocks with high TOC contents and a high hydrocarbon generation potential ($S_1 + S_2$). The authors believe that the high organic matter abundance of the Ha'erjiawu Formation shales may be related to volcanic hydrothermal activity and terrestrial organic matter inputs, which collectively contributed to high paleoproductivity in the surface water.

5.3.1 Hydrothermal activities

During the deposition of the Ha'erjiawu Formation in the Malang Sag, volcanic eruptions were frequent, and volcanic rocks are widely distributed. The formation is dominated by volcanic rocks interbedded with organic-rich rocks. The thermal driving force was caused by the volcanic eruptions, and the deposition of volcanic ash forms an active heat flux circulatory system. As a result, the sedimentary water column was non-hydrostatic, non-reducing and had almost no water stratification (Shan et al. 2013; Jin 1998; Jin et al. 1999, 2006). This is consistent with the analysis of the trace element concentrations and biomarker compounds. The hydrothermal activity generated by the volcanic eruption resulted in some of the transition metals being anomalously enriched (Table 6), such as V, Ni, Cu, and Zn. The transition metal contents of the source rocks are similar to those of volcanic rocks, and the contents of some of the samples are even significantly higher than those of volcanic rocks. This indicates that the transition metals in the volcanic rocks were extracted from the surrounding source rocks, and the migration of the transition metals is significant. The

Table 6 Comparison of the transition metals contents of the source rocks and volcanic rocks (unit, ppm)

Sample	M71-5	M68-2	M361-1	M361-2	M40	M40	ND201	ND201	ND201
	Organic-rich rocks				Tuff	Volcanic rock	Tuff	Tuff	Tuff
Li	29.3	13.5	9.52	5.49	11.27	4.58	8.05	12.65	9.45
Sc	16	25	8.09	7.74	2.68	1.97	22.09	21.38	21.72
V	197	522	323	467	50.08	188	198	183	181
Cr	76	125	22.1	29.5	35.72	97.98	132	123	121
Ni	38.6	63.7	18.6	24.1	40.07	29	27.89	29.85	28.72
Cu	59.9	163	47.2	92.2	31.67	101	66.02	59.89	63.32
Zn	97.6	159	66.1	95.2	184	86.09	96.49	75.99	100
Ga	22.8	22	12.8	9.8	5.87	24.22	22.04	20.62	20.8
Sr	308	1094	230	215	66.25	507	1926	2143	1975
Y	30.1	23.5	20.7	15.5	7.59	3.21	25.22	27.73	27.4
Zr	230	291	134	116	411	410	462	399	421

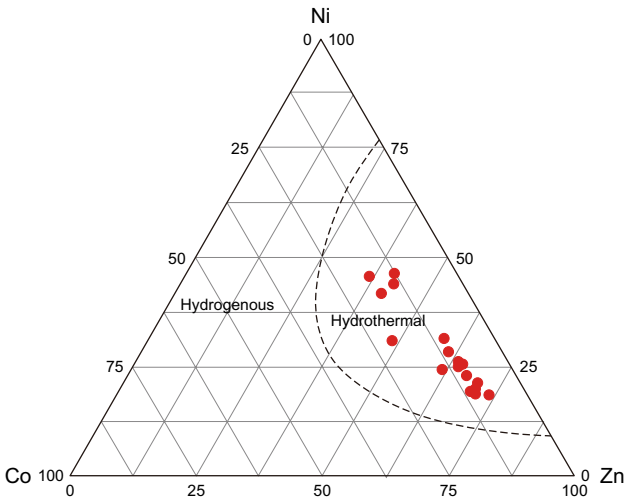

Fig. 14 Co versus Ni versus Zn ternary diagram after Choi and Hariya (1992)

transition metals have an important role in promoting algae/bacteria blooms (Jin et al. 2006; Wang et al. 2013b). Therefore, the enrichment of these metals reflects hydrothermal inputs during the deposition of the Ha'erjiawu Formation. In addition, in the ternary diagrams of Ni versus Co versus Zn (Fig. 14), all the samples fall in the hydrothermal sediment zone, which also indicates that the Ha'erjiawu Formation was deposited in a hydrothermal environment.

Hydrothermal activity is usually closely linked to life activities and microorganism bloom (Zhang et al. 2006b; Wang et al. 2013b; Westall et al. 2015). Hydrothermal activity also provides a large amount of minerals and nutrients to the water column, which promotes the enrichment of organisms and increases the organic matter content of the water column (Jin et al. 2006; Callac et al. 2013; Wang et al. 2013b). Previous studies have demonstrated that the Cr/Zr ratio and transition metals concentrations (Zn, Cu, and so on) are useful indicators of the intensity of the hydrothermal input (Marchig et al. 1982; Pujol et al. 2006). As shown in Fig. 15, the slightly positive correlations between TOC content and the Cr/Zr ratio or the Zn content indicate that hydrothermal activity contributed to organic matter enrichment during deposition of the Ha'erjiawu Formation. The above ambiguity correlations suggest the contribution of the hydrothermal input to the organic matter enrichment may have been affected by other factors, such as the terrigenous nutrient supply. Interestingly, the formation of organic-rich rocks associated with hydrothermal activity has been reported in non-marine basins in China, including the Lucaogou Formation in the Santanghu Basin (Zhang et al. 2018) and the Fengcheng and Lucaogou Formations in the Junggar Basin (Cao et al. 2015). Therefore, as a nutrient source, hydrothermal activities strongly controlled the development of aquatic organisms. Moreover, in the area far away from the volcanic edifice, life activities and microorganism blooms may have consumed a lot of oxygen in the water column, causing intermittent anoxic conditions, which was also beneficial to the preservation of organic matter. These processes collectively contributed to the formation of organic-rich rocks.

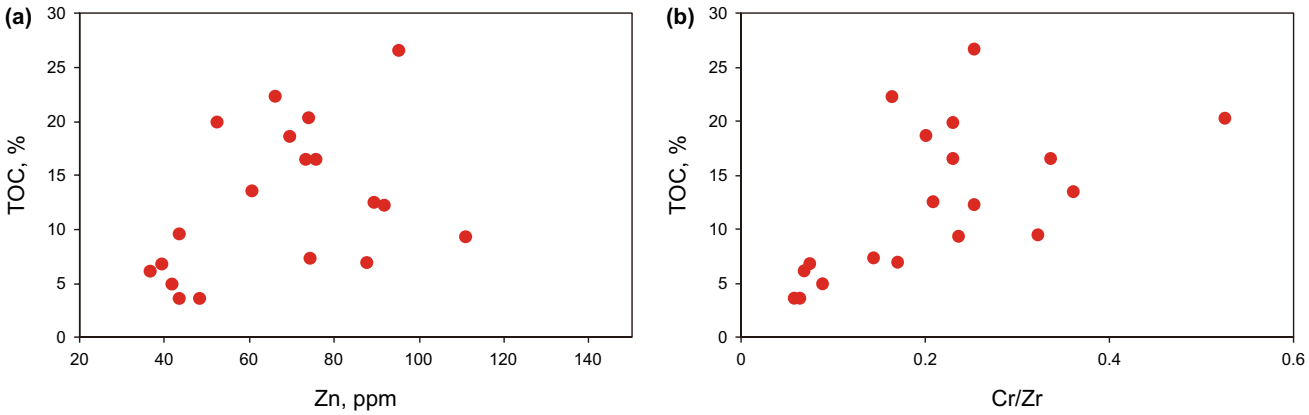

Fig. 15 Plot of **a** TOC versus Zn content and **b** TOC versus Cr/Zr ratio

5.3.2 Terrigenous organic matter input

The analysis results of the Ha'erjiawu Formation shales show that the TOC content is positively correlated with the siliceous mineral content, but it is negatively correlated with the carbonate mineral content (Fig. 16a, b). The silicate mineral content and the carbonate content usually reflect the terrigenous input from a river system and carbonate production in lacustrine basins, respectively (Zhang et al. 2018). The

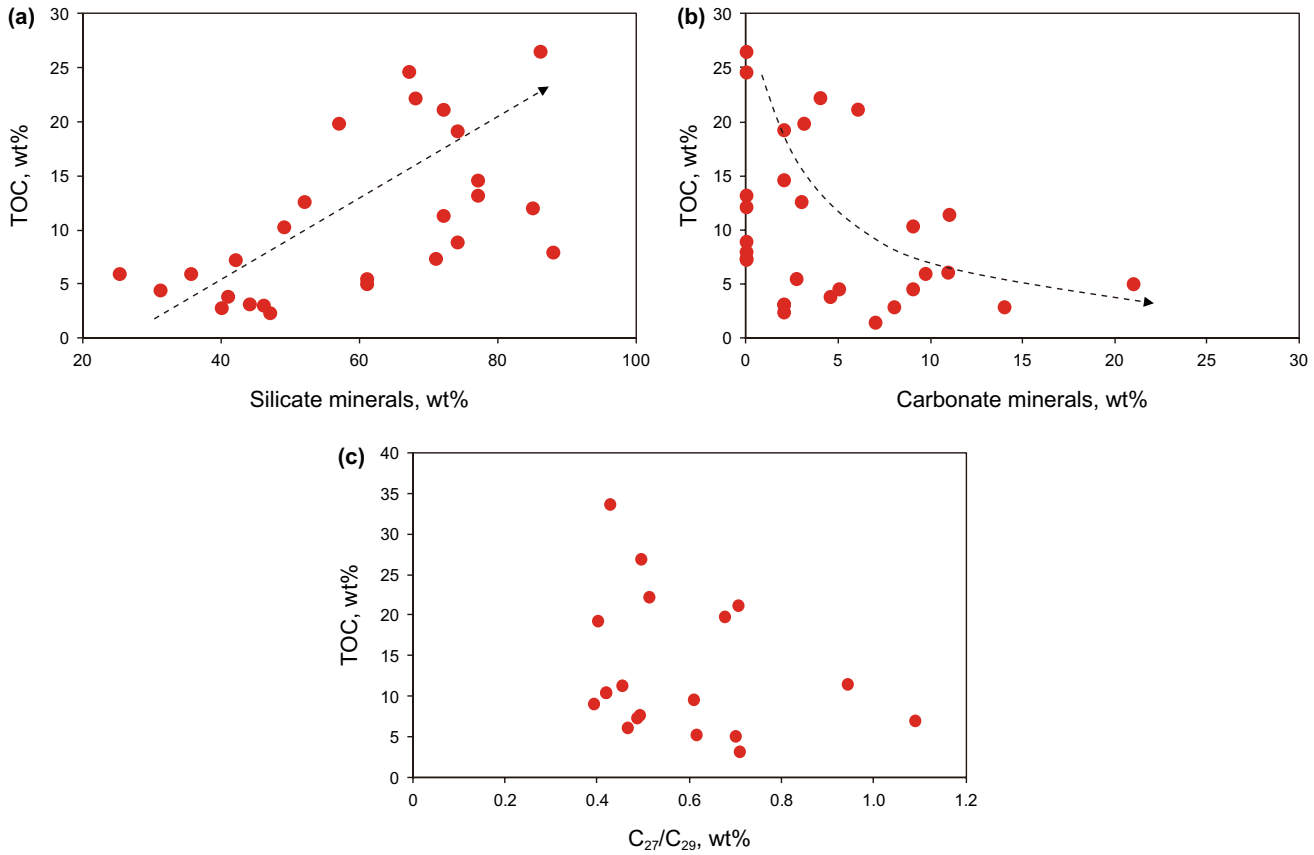

Fig. 16 Plots of **a** TOC versus siliceous mineral content, **b** TOC versus carbonate mineral content, **c** TOC versus C_{27}/C_{29} ratio

positive correlation between the siliceous mineral content and the total organic carbon (TOC) content indicates that the terrigenous input promoted the organic matter enrichment. The major reason for this is that the nutrient input increased with increasing siliceous mineral content. Adequate nutrients supply can promote the reproduction of organisms in lakes. In addition, the terrigenous input brings abundant land plant organic matter and nutrients supply, which collectively increases the productivity in the water column and facilitating the enrichment of organic matter (Littke et al. 1991). In contrast, the negative correlation between the carbonate mineral content and TOC content indicates that the carbonate constituents had a significant dilution effect on the organic matter enrichment during the deposition of the Ha'erjiawu Formation.

The contents of the C_{27} regular steranes and the C_{29} regular steranes reflect the source of the organic matter. A higher C_{27} regular sterane content often represents the significant contribution of plankton or algae in the water column, while a higher C_{29} regular sterane content reflects the higher input of land plant organic matter (Ding et al. 2015; Song et al. 2017). In this study, the ratio of the C_{27} regular steranes to the C_{29} regular steranes ($\omega(C_{27})/\omega(C_{29})$) reflects the supply intensity of the terrigenous organic matter. The higher values correspond to a lower input of terrigenous organic matter. The relationship between $\omega(C_{27})/\omega(C_{29})$ and ω(TOC) is illustrated in Fig. 16c, and the results show a weakly negative correlation. The ω(TOC) of the source rocks decreases with increasing of $\omega(C_{27})/\omega(C_{29})$. The input of terrigenous organic matter has a certain control on the formation of high-quality source rocks.

5.4 Unconventional hydrocarbon potential

Using TOC and Rock–Eval data shows that the Ha'erjiawu Formation organic-rich rocks have a good to very good potential to generate conventional oil (Table 3, Fig. 6). Many wells in the overlying strata have obtained commercial oil production (such as the Carboniferous Kalagang Formation and the upper member of the Ha'erjiawu Formation), which have been shown to be derived from the Ha'erjiawu Formation (Liu et al. 2015; Huang et al. 2012). Furthermore, according to organic geochemical and mineralogical data, we investigated whether the organic-rich rocks of the Ha'erjiawu Formation also have a good potential for shale oil exploration. Jarvie (2012) proposed using an oil

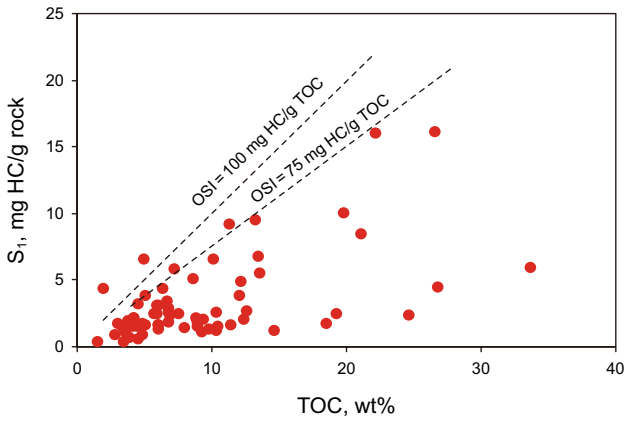

Fig. 17 S_1 versus TOC indicating movable oil content of the Ha'erjiawu Formation in the Santanghu Basin

saturation index OSI (S_1/TOC × 100) to evaluate shale oil potential. When the OSI is > 100 mg HC/g TOC, there is an oil crossover phenomenon, which suggests that the shale oil is movable. It is generally recognized that OSI values of 75–100 mg HC/g TOC represent a potential shale oil target with abundant absorbed hydrocarbons. In this study, the OSI values of the Ha'erjiawu Formation vary from 8.22 to 228.35 mg HC/g TOC, with an average of 43.25 mg HC/g TOC. The OSI values of most of the organic-rich rock samples are < 100 mg HC/g TOC, with only five samples having values higher than 75 mg HC/g TOC (Fig. 17). These results indicate that the Ha'erjiawu Formation has a poor shale oil potential. The major reason for this may be that the high TOC and clay mineral contents of the Ha'erjiawu Formation lead to a strong adsorption capacity of hydrocarbon fluids, which is not conducive to the shale fracking of and the outflow of hydrocarbon fluids. Therefore, the organic-rich rocks of Ha'erjiawu Formation are good potential hydrocarbon-generating source rocks, but they are not suitable for shale oil exploration and development.

6 Conclusions

Using the petrology (pyrite size, carbonate and siliceous content), organic and inorganic geochemical indicators (Pr/Ph, gammacerane, V/Cr, V/(V + Ni) and Sr/Ba, Rb/K, B/Ga, and B content) reconstruct the paleoenvironment of the Ha'erjiawu Formation in the Santanghu Basin. Furthermore, we discuss the main influence factors of organic matter enrichment in the high-quality source rocks of the Ha'erjiawu Formation. The main conclusions are as follows:

1. The high organic matter abundance source rocks of the Ha'erjiawu Formation were deposited in freshwater-mildly brackish and warm-humid environments. The Ha'erjiawu Formation received hydrothermal input during the sedimentary process, which resulted in complex redox conditions. The Ha'erjiawu Formation also experienced episodic transitions between dysoxic and anoxic depositional environments, but predominantly had a dysoxic environment.
2. Under the background of volcanic eruptions, the primary productivity in the surface water contributed to the organic matter enrichment of the Ha'erjiawu Formation. The terrigenous organic matter input and hydrothermal activity were conductive to improving the paleoproductivity, with transient anoxic conditions during volcanic intermission, which promoted organic matter accumulation.
3. According to organic matter abundance, organic matter type and maturity, the source rocks of Ha'erjiawu Formation have good to very good hydrocarbon generation potential. The OSI values of the Ha'erjiawu Formation shale are low, indicating that it contains a large amount of non-movable oil. These results indicate that the Ha'erjiawu Formation is not suitable for shale oil exploration and development.

Acknowledgements This work is financially supported by the National Natural Science Foundation of China (Grant No. 41472111, 41702127). We thank PetroChina Tuha Oilfield Company for kindly providing subsurface datasets, and the Liu Juntian Senior Engineer of Tuha Oilfield Company for providing assistance and guidance and for the permission to publish the results of this study. We thank LetPub (www.letpub.com) for its linguistic assistance during the preparation of this manuscript.

References

Banerjee I, Goodarzi F. Paleoenvironment and sulfur-boron contents of the Mannville (Lower Cretaceous) coals of southern Alberta. Canada. Sediment Geol. 1990;67:297–310. https://doi.org/10.1016/0037-0738(90)90040-z.

Canuel EA, Freeman KH, Wakeham SG. Isotopic Compositions of Lipid Biomarker Compounds in Estuarine Plants and Surface Sediments. Limnol Oceanogr. 1997;42:1570–83. https://doi.org/10.4319/lo.1997.42.7.1570.

Campbell GDWFA. Chemical Composition of Shales of Mannville Formation (Lower Cretaceous) of Central Alberta, Canada. AAPG Bull. 1965;49:81–7. https://doi.org/10.1306/a66334ea-16c0-11d7-8645000102c1865d.

Cao J, Lei DW, Li YW, et al. Ancient high-quality alkaline lacustrine source rocks discovered in the Lower Permian Fengcheng Formation, Junggar Basin. Acta Pet. Sin. 2015;36:781–90. https://doi.org/10.7623/syxb201507002 **(in Chinese)**.

Collister JW, Lichtfouse E, Hieshima G, et al. Partial resolution of sources of n-alkanes in the saline portion of the Parachute Creek Member, Green River Formation (Piceance Creek Basin, Colorado). Org Geochem. 2007;21:645–59. https://doi.org/10.1016/0146-6380(94)90010-8.

Choi JH, Hariya Y. Geochemistry and depositional environment of Mn oxide deposits in the Tokoro Belt, northeastern Hokkaido, Japan. Econ Geol. 1992;87:1265–74. https://doi.org/10.2113/gsecongeo.87.5.1265.

Callac N, Rommevaux JC, Rouxel O, et al. Microbial colonization of basaltic glasses in hydrothermal organic-rich sediments at Guaymas Basin. Front Microbiol. 2013;4:250. https://doi.org/10.3389/fmicb.2013.00250.

Ding XZ, Liu GD, Huang ZL, et al. Source rock distribution and formation in Saihantala depression, Erlian Basin. J Cent South Univ: Nat Sci Ed. 2015;46:1739–46. https://doi.org/10.11817/j.issn.1672-7207.2015.05.023 **(in Chinese)**.

Didyk B, Simoneit BRT, Brassell SC, et al. Organic geochemical indicators of palaeoenvironmental conditions of sedimentation. Nature. 1978;272:216–22. https://doi.org/10.1038/272216a0.

Demaison GJ, Moore GT. Anoxic environments and oil source bed genesis. AAPG Bull. 1980;2:9–31. https://doi.org/10.1306/2f91945e-16ce-11d7-8645000102c1865d.

Espitalié J, Marquis F, Barsony I. Geochemical logging. In: Voorhess KJ, editor. Analytical Pyrolysis. Boston: Butterworths; 1984. p. 53–79. https://doi.org/10.1016/b978-0-408-01417-5.50013-5.

Fan YH, Qu HJ, Wang H, et al. The application of trace elements analysis to identifying sedimentary media environment: a case study of Late Triassic strata in the middle part of western Ordos Basin. Geol Chin. 2012;39:382–9. https://doi.org/10.1016/j.still.2012.05.017 **(in Chinese)**.

Farhaduzzaman M, Abdullah WH, Islam MA. Depositional environment and hydrocarbon source potential of the Permian Gondwana coals from the Barapukuria Basin, Northwest Bangladesh. Int J Coal Geol. 2012;90–91:162–79. https://doi.org/10.1016/j.coal.2011.12.006.

Gallego-Torres D, Reolid M, Nieto-Moreno V, et al. Pyrite framboid size distribution as a record for relative variations in sedimentation rate: an example on the Toarcian Oceanic Anoxic Event in Southiberian Palaeomargin. Sediment Geol. 2015;330:59–73. https://doi.org/10.1016/j.sedgeo.2015.09.013.

Gamero-Diaz H, Miller C, Lewis R. sCore: a mineralogy based classification scheme for organic mudstones. In: SPE Annual Technical Conference and Exhibition, New Orleans, Louisiana, USA. Paper SPE-166284, 2013. https://doi.org/10.2118/166284-ms.

GB/T 19145-2003. Determination of total organic carbon in sedimentary rock (in Chinese).

GB/T 18606-2001. The standard test method for biomarker in sediment and crude oil by GC-MS (in Chinese).

GB/T 14506.30-2010. Methods for chemical analysis of silicate Rocks-Part 30: Determination of 44 elements (in Chinese).

Ghassal BI, Littke R, Atfy HE, et al. Source rock potential and depositional environment of Upper Cretaceous sedimentary rocks, Abu Gharadig Basin, Western Desert, Egypt: an integrated palynological, organic and inorganic geochemical study. Int J Coal Geol. 2018;186:14–40. https://doi.org/10.1016/j.coal.2017.11.018.

Gomes A, Saha A, Chatterjee I, Chakravarty AK. Viper and cobra venom neutralization by β-sitosterol and stigmasterol isolated from the root extract of Pluchea indica Less. (Asteraceae). Phytomedicine. 2007;1:637–43. https://doi.org/10.1016/j.phymed.2006.12.020.

Goossens H, Leeuw JWD, Schenck PA, et al. Tocopherols as likely precursors of pristane in ancient sediments and crude oils. Nature. 1984;312:440–2. https://doi.org/10.1038/312440a0.

Huang WY, Meinschein WG. Sterols as ecological indicators. Geochim Cosmochim Acta. 1979;43:739–45. https://doi.org/10.1016/0016-7037(79)90257-6.

Huang ZL, Liu B, Luo QS, et al. Main controlling factors and models of carboniferous volcanic hydrocarbon accumulation in the Malang Sag, Santang Basin. Acta Geol Sin. 2012;86:1210–6. https://doi.org/10.3969/j.issn.0001-5717.2012.08.004 **(in Chinese)**.

Hu WS. Tectonic evolution and petroleum systems of Santanghu Basin, Xinjiang. J. Southwest-China Petroleum Instit. 1997;19:14–20. https://doi.org/10.3863/j.issn.1000-2634.1997.02.04 **(in Chinese)**.

Hu D, Rao S, Wang ZT, et al. Thermal and maturation history for Carboniferous source rocks in the Junggar Basin, Northwest China: implications for hydrocarbon exploration. Pet. Sci. 2020;17:36–50. https://doi.org/10.1007/s12182-019-00392-2.

Hatch JR, Leventhal JS. Relationship between inferred redox potential of the depositional environment and geochemistry of the Upper Pennsylvanian (Missourian) Stark Shale Member of the Dennis Limestone, Wabaunsee County, Kansas, U.S.A. Chem Geol. 1992;99:65–82. https://doi.org/10.1016/0009-2541(92)90031-y.

Jones B, Manning DAC. Comparison of geochemical indices used for the interpretation of paleoredox conditions in ancient mudstones. Chem Geol. 1994;111:111–29. https://doi.org/10.1016/0009-2541(94)90085-x.

Jarvie DM. Shale resource systems for oil and gas: part 2—shale-oil resource systems. In: Breyer, J.A. (Ed.), Shale Reservoirs—Giant Resources for the 21st Century. AAPG Memoir 97. 2012; pp. 89–119. https://doi.org/10.1306/13321447m973489.

Jia C, Huang J, Kershaw S, et al. Microbial response to limited nutrients in shallow water immediately after the End-Permian mass extinction. Geobiology. 2012;10:60–71. https://doi.org/10.1111/j.1472-4669.2011.00310.x.

Jin Q. Hydrocarbon Generation in rift basins, Eastern China: catalysis and Hydrogenation-Interaction between volcanic minerals and organic matter. Adv Earth Sci. 1998;13:39–46. https://doi.org/10.1002/cjoc.200890146 **(in Chinese)**.

Jin Q, Zhai QL. Volcanic and thermal-water activities and hydrocarbon generations in the rift basins. Eastern China. Chinese J. Geol. 2003;38:413–24. https://doi.org/10.3321/j.issn:0563-5020.2003.03.008.

Jin Q, Xiong SS, Lu PD, et al. Catalysis and hydrogenation: volcanic activity and hydrocarbon generation in rift basins, eastern China. Appl Geochem. 1999;14:547–58. https://doi.org/10.1016/s0883-2927(98)00086-9 **(in Chinese)**.

Jin Q, Wan CL, Zhou FX, et al. Migration of trace elements from basalts to oil source rocks and its geological significance in Minqiao area of Jinhu depression. J Chin Univ Pet. 2006;30:1–5. https://doi.org/10.1007/s11769-006-0378-6 **(in Chinese)**.

Katz BJ. Controls on distribution of lacustrine source rocks through time and space. Lacustrine Basin Exploration-Case Studies Modern Analogs. 1990;50:61–76. https://doi.org/10.1306/m50523c4.

Kendall CGSC, Alsharhan AS, Jarvis I. Evaporitic source rocks: mesohaline responses to cycles of "famine or feast" in layered brines[M]//Quaternary carbonate and evaporite sedimentary facies and their ancient analogues: A Tribute to Douglas James Shearman. Wiley. 2012; vol 43, pp. 315–92. https://doi.org/10.1002/9781444392326.ch16.

Kryc KA, Murray RW, Murray DW. Al-to-oxide and Ti-to-organic linkages in biogenic sediment: relationships to paleo-export production and bulk Al/Ti. Earth Planet Sci Lett. 2003;211:125–41. https://doi.org/10.1016/s0012-821x(03)00136-5.

Liu B, Jia MC, Huang ZL, et al. Identification and prediction of source rocks in Carboniferous volcanic systems in Malang Sag, Santanghu Basin. Pet Geol Exp. 2015;37:452–9. https://doi.org/10.11781/sysydz201504452 **(in Chinese)**.

Liu B, Bechtel A, Sachsenhofer RF, et al. Depositional environment of oil shale within the second member of Permian Lucaogou Formation in the Santanghu Basin, Northwest China. Int J Coal Geol. 2017;175:10–25. https://doi.org/10.1016/j.coal.2017.03.011.

Li H, Lu JL, Li RL, et al. Generation Paleoenvironment and its controlling factors of lower cretaceous lacustrine hydrocarbon source rocks in Changling Depression, South Songliao Basin. Earth Sci. 2017;42:1774–86. https://doi.org/10.3799/dqkx.2017.539 **(in Chinese)**.

Liu JT, Liu YP, Guo MZ, et al. Volcanic reservoir characteristics and genetic mechanism of Carboniferous in Niudong area of Santanghu Basin. Lithol. Reservoirs. 2009;21:64–9. https://doi.org/10.3969/j.issn.1673-8926.2009.02.013 **(in Chinese)**.

Littke R, Leythaeuser D, Rullkotter J, et al. Keys to the depositional history of the Posidonia Shale (Toarcian) in the Hils Syncline, northern Germany. Geol. Soc. Lond. Special Publ. 1991;58:311–33. https://doi.org/10.1144/gsl.sp.1991.058.01.20.

Liu JT, Liang H, Hou QZ, et al. Paleosalinity recovering of environment deposition in Late Carboniferous of Santanghu Basin. Xinjiang Oil Gas. 2011;1:26–8. https://doi.org/10.1007/bf00267652 **(in Chinese)**.

Lin KX, Li YB, Gong WP, et al. Geochemical characteristics of upper Palaeozoic volcanic rocks and their tectonic settings in the Santanghu Basin, Xinjiang. Geol J Univ. 1997;3:202–11. https://doi.org/10.16108/j.issn1006-7493.1997.02.008 **(in Chinese)**.

Liu G, Zhou DS. Application of microelements analysis in identifying sedimentary environment-taking Qianjiang formation in the Jianghan Basin as an example. Pet Geol Exp. 2007;29:307-306. https://doi.org/10.11781/sysydz200703307 **(in Chinese)**.

Li JL, Chen DJ. Summary of quantified research method on paleosalinity. Petroleum Geol. Recovery Efficiency. 2003;10:1–3. https://doi.org/10.3969/j.issn.1009-9603.2003.05.001 **(in Chinese)**.

Li YT, Huang ZL, An CL, et al. Characteristics and differences of source rocks in the lower and upper members of Carboniferous Ha'erjiawu Formation in the Malang Sag of the Santanghu Basin, NW China. Nat Gas Geosci. 2018;29:73–86 **(in Chinese)**.

Lu HO, Yuan BQ, Li YH, et al. Characteristics of Fault Structures in Santanghu Basin. Xinjiang Pet Geol. 2012;33:293–6. https://doi.org/10.11764/j.issn.1672-1926.2017.09.011 **(in Chinese)**.

Marchig V, Gundlach H, Möller P, et al. Some geochemical indicators for discrimination between diagenetic and hydrothermal metalliferous sediments. Mar Geol. 1982;50:241–56. https://doi.org/10.1016/0025-3227(82)90141-4.

Mackenzie AS, Brassell SC, Eglinton G, et al. Chemical fossils: the geological fate of steroids. Science. 1982;217:491–504. https://doi.org/10.1126/science.217.4559.491.

Mello MR, Telnaes N, Gaglianone PC, Chicarelli MI, Brassell SC, Maxwell JR. Organic geochemical characterisation of depositional palaeoenvironments of source rocks and oils in Brazilian marginal basins. Organ. Geochem. 1988;13(1–3):31–45. https://doi.org/10.1016/0146-6380(88)90023-X.

Meyers PA, Arnaboldi M. Trans-Mediterranean comparison of geochemical paleoproductivity proxies in a mid-Pleistocene interrupted sapropel. Paleogeogr Paleoclimatol Paleoecol. 2005;222:313–28. https://doi.org/10.1016/j.palaeo.2005.03.020.

Morford JL, Emerson S. The geochemistry of redox sensitive trace metals in sediments. Geochim Cosmochim Acta. 1999;63:1735–50. https://doi.org/10.1016/s0016-7037(99)00126-x.

Magoon LB, Dow WG. The Petroleum System from Source to Trap. AAPG Memoir. 1991;14:627. https://doi.org/10.1016/0920-4105(95)00059-3.

McLennan SM. Relationships between the trace element composition of sedimentary rocks and upper continental crust. Geochem Geophys Geosyst. 2001;2(4):203–36. https://doi.org/10.1029/2000gc000109.

Pujol F, Berner Z, Stüben D, et al. Paleoenvironmental changes at the Frasnian/Famennian boundary in key European sections: chemostratigraphic constraints. Paleogeogr Paleoclimatol Paleoecol. 2006;240:120–45. https://doi.org/10.1016/j.palaeo.2006.03.055.

Peters KE. Guidelines for evaluating petroleum source rock using programmed pyrolysis. AAPG Bull. 1986;70:318–29. https://doi.org/10.1306/94885688-1704-11d7-8645000102c1865d.

Peters KE, Moldowan, JM. The Biomarker Guide: Interpreting Molecular Fossils in Petroleum and Ancient Sediments. Prentice Hall, Englewood Cliffs, New Jersey. 1993. 550-90. https://doi.org/10.1017/cbo9780511524868.

Qin JZ. Hydrocarbon source rocks of China. Beijing: Science Press; 2015 **(in Chinese)**.

Ren JL, Zhang J, Liu SM. A review on aluminum to titanium ratio as a geochemical proxy to reconstruct paleoproductivity. Adv Earth Sci. 2005;20:1314–20. https://doi.org/10.1111/j.1745-7254.2005.00209.x **(in Chinese)**.

Shan XL, Li JY, Chen SM, et al. Subaquatic volcanic eruptions in continental facies and their influence on high quality source rocks shown by the volcanic rocks of a faulted depression in Northeast China. Sci. China Earth Sci. 2013;56:1926–33. https://doi.org/10.1007/s11430-013-4657-7 **(in Chinese)**.

Schoell M, Hwang RJ, Carlson RMK, et al. Carbon isotopic composition of individual biomarkers in gilsonites (Utah). Org Geochem. 1994;21:673–83. https://doi.org/10.1016/0146-6380(94)90012-4.

Sun ZM, Xiong BX, Li YL, et al. Structural characteristics and favorable belt for hydrocarbon exploration in Santanghu Basin. Pet Geol Exp. 2001;23:23–6. https://doi.org/10.3969/j.issn.1001-6112.2001.01.004 **(in Chinese)**.

Song Y, Bechtel A, Sachsenhofer RF, et al. Depositional environment of the Lower Cretaceous Muling Formation of the Laoheishan Basin (NE China): implications from geochemical and petrological analyses. Org Geochem. 2017;104:19–34. https://doi.org/10.1016/j.orggeochem.2016.11.008.

Simoneit BRT, Leif RN, Neto FRDA, et al. On the presence of tricyclic terpane hydrocarbons in permian tasmanite algae. Naturwissenschaften. 1990;77:380–3. https://doi.org/10.1007/bf01135736.

Tissot B, Welte D. Petroleum formation and occurrence. Springer-Verlag. Earth-Sci Rev. 1980;16:372–3. https://doi.org/10.1016/0012-8252(80)90071-9.

Volkman JK, Maxwell JR. Acyclic isoprenoids as biological markers. In: Johns RB, editor. Biological Markers in the Sedimentary Record. Elsevier: Amsterdam; 1986. p. 1–42.

Wang PK, Huang YJ, Wang CS, et al. Pyrite morphology in the first member of the Late Cretaceous Qingshankou Formation, Songliao Basin, Northeast China. Paleogeogr Paleoclimatol Paleoecol. 2013a;385:125–36. https://doi.org/10.1016/j.palaeo.2012.09.027.

Wang SR, Song DF, He DF. The enrichment effect of organic materials by volcanic ash in sediments of the Santanghu Basin and the evolutionary pattern of tuffaceous source rocks. Acta Pet Sin. 2013b;34:1077–87. https://doi.org/10.7623/syxb201306006 **(in Chinese)**.

Walker NBPCT. Departure Curves for Computing Paleosalinity from Boron in Illites and Shales. AAPG Bull.1963; 47: 833-41. https://doi.org/10.1306/bc743a93-16be-11d7-8645000102c1865d.

Wu XZ, Qi XF, Tang Y, et al. Carboniferous strata and lithofacies paleogeography & source rock in Northern Xinjiang. Geoscience. 2008;22:549–57. https://doi.org/10.3969/j.issn.1000-8527.2008.04.009 **(in Chinese)**.

Wilkin RT, Barnes HL, Brantley SL. The size distribution of framboidal pyrite in modern sediments: an indicator of redox conditions.

Geochim Cosmochim Acta. 1996;60:3897–912. https://doi.org/10.1016/0016-7037(96)00209-8.

Westall F, Campbell KA, Breheret JG, et al. Archean (3.33 Ga) microbe-sediment systems were diverse and flourished in a hydrothermal context. Geology. 2015;43:615–8. https://doi.org/10.1130/g36646.1.

Xiao XM, Wei Q, Gai HF, et al. Main controlling factors and enrichment area evaluation of shale gas of the Lower Paleozoic marine strata in south China. Pet. Sci. 2015;12:573–86. https://doi.org/10.1007/s12182-015-0057-2.

Ye CC, Yang YB, Fang XM, et al. Late Eocene clay boron-derived paleosalinity in the Qaidam Basin and its implications for regional tectonics and climate. Sediment Geol. 2016;346:49–59. https://doi.org/10.1016/j.sedgeo.2016.10.006.

Zhang ZL, Wu LY, Shu NZ, et al. Cause analysis of abnormal Tmax values on Rock-Eval pyrolysis. Pet Explor Dev. 2006a;33(1):72–5 **(in Chinese)**. https://doi.org/10.3321/j.issn:1000-0747.2006.01.016.

Zhang WZ, Yang H, Li JF, et al. Leading effect of high-class source rock of Chang 7 in Ordos Basin on enrichment of low permeability oil-gas Accumulation-Hydrocarbon generation and expulsion mechanism. Pet Explor Dev. 2006b;33:289–93. https://doi.org/10.3321/j.issn:1000-0747.2006.03.006 **(in Chinese)**.

Zhang SH, Liu CY, Liang H, et al. Paleoenvironmental conditions, organic matter accumulation, and unconventional hydrocarbon potential for the Permian Lucaogou Formation organic-rich rocks in Santanghu Basin, NW China. Int J Coal Geol. 2018;185:44–60.

Zhao ZH, Guo ZJ, Zhang C, et al. Tectonic Evolution of the Santanghu Basin, East Xinjiang and Its Implication for the Hydrocarbon Accumulation. Acta Scicentiarum Naturalum Universitis Pekinesis. 2003;39:219–28. https://doi.org/10.3321/j.issn:0479-8023.2003.02.012 **(in Chinese)**.

Zhang ZH, Yang F, Li DM, et al. The organic Geochemistry research progress in cenozoic salaried lake in China. Adv Earth Sci. 2000;15:65–70. https://doi.org/10.11867/j.issn.1001-8166.2000.01.0065 **(in Chinese)**.

Zou HY, Zhou XH, Hao F, et al. Oil origin analysis of PL19-3 Oil Field, Bozhong area and its significance to oil accumulation and exploration. J Xi'an Shiyou Univ. 2009;24:13–6. https://doi.org/10.3969/j.issn.1673-064x.2009.01.003 **(in Chinese)**.